MSW MANAGEMENT -Multidisciplinary, Scientific Work and Management Journal
ISSN: 1053-7899
Vol. 35 Issue 2, 2025, Pages: 597-630

DRAGONFLY SWARM INTELLIGENCE ENHANCED SEMI SUPERVISED GENERATIVE ADVERSARIAL NETWORK FOR RETINAL FEATURE OPTIMIZATION

D. Pavithra
Research Scholar Department of Computer Science
PSG College of Arts & Science
Coimbatore, India
pavikoki555@gmail.com

Dr. K. Padmavathi
Associate Professor
Department of Computer Science
PSG College of Arts & Science Coimbatore, India padmasakthivel@gmail.com

Abstract:

Automated diabetic retinopathy analysis demands models capable of high reliability under sparse supervision, where conventional supervised architectures often fail to generalise across limited annotated data. The present study introduces Dragonfly Swarm Optimised Semi Supervised Generative Adversarial Network (DSO-SSGAN), a biologically inspired framework designed for robust multi-stage retinal image classification. The approach integrates dragonfly swarm intelligence into the latent generative process, regulating search trajectories, enhancing feature diversity, and stabilising convergence within adversarial learning. A semi-supervised architecture combines confidence-based filtering, domain alignment, and progressive curriculum scheduling to align labelled and unlabelled representations. The model is trained and validated on the Diabetic Retinopathy Dataset, achieving an accuracy of 77.512%, surpassing conventional semi-supervised baselines with consistent gradient stability and reduced overfitting. Interpretability is strengthened through latent traversal analysis that visualises class transitions and reinforces clinical traceability. The unified framework demonstrates computational resilience and adaptive visual encoding under limited supervision, positioning swarm-driven latent optimisation as an efficient strategy for scalable diabetic retinopathy classification and future medical image intelligence systems.

Keywords:

Swarm Intelligence, Adversarial Learning, Latent Space, Optimization, Retinopathy, GAN

MSW MANAGEMENT -Multidisciplinary, Scientific Work and Management Journal
ISSN: 1053-7899
Vol. 35 Issue 2, 2025, Pages: 597-630

1. INTRODUCTION

Diabetes mellitus continues to be one of the most prevalent metabolic conditions worldwide, with a steep increase across both urban and rural populations [1]. Long-term exposure to elevated glucose levels contributes to vascular damage across multiple organs. Visual impairment caused by diabetic retinopathy represents a profound secondary effect of this condition [2]. Retinal abnormalities can emerge without warning, leading to unnoticed vision loss unless monitored. Small blood vessels in the retina begin to leak or swell, forming microaneurysms, cotton-wool spots, or neovascular growths. These pathological changes progress in stages and eventually interfere with central vision [3]. Clinical examination typically involves fundus photography and a manual grading process conducted by trained professionals. The increasing scale of diabetic patients continues to place significant demand on ophthalmic diagnostic resources. The limited availability of retinal specialists underscores the need for intelligent screening solutions that can operate with high consistency across large volumes of retinal image data [4].

Supervised learning architectures have been widely adopted for image-based detection and classification tasks in healthcare. Diabetic retinopathy, with its clearly visible morphological indicators, has been a suitable condition for evaluating these models [5]. Deep convolutional networks extract low-level and high-level spatial features, identifying lesions and abnormalities that are sometimes not easily visible to the human eye. Learning frameworks have been developed to predict disease presence and severity grade based on image patterns and localization [6], [7]. Precision in class-specific identification depends on balanced and representative training datasets. Complexities arise in classification tasks involving multiple severity stages, especially where early signs are visually subtle [8]. Limited availability of annotated datasets introduces further constraints on training coverage. Overfitting to high-frequency stages or confusion between adjacent classes can reduce predictive integrity [9]. Shifts in lighting, resolution, and capture methods further impact generalization across different imaging sources or population subgroups [10], [11].

Optimization techniques derived from biological phenomena provide an alternative approach to addressing learning inconsistencies in medical image models [12]. Behavioural processes found in natural systems often serve as templates for adaptive search and decision rules. Swarm-inspired algorithms operate through agent-based coordination, where individual units move according to rules shaped by local interactions. Such behaviour supports distributed control and spatial diversity [13]. Integration with classification systems enables selective sampling, dynamic weight updates, and balanced feature learning, allowing for more effective learning. Adaptive agents modify search directions in response to feedback rather than relying on fixed gradients. This supports movement toward better-performing solution spaces across training epochs [14]. Algorithms inspired by fish schooling, bird flocking, or insect navigation have been applied in feature reduction, data generation, and parameter tuning tasks [15], [16]. Dragonfly-based modelling, derived from visual hunting patterns, captures five types of social forces that influence movement: alignment, cohesion, separation, food attraction, and predator avoidance. These components make the structure suitable for guiding latent representations in classification-oriented pipelines.

Learning architectures configured to incorporate both supervised and unsupervised data have gained attention for diagnostic imaging. In contexts where annotated datasets are limited, semi-supervised approaches enable the model to access a broader range of data variations. Synthetic data generation further supports diversity and representation across all stages of the condition [17]. Adversarial learning introduces a framework where sample quality and class relevance are enforced simultaneously. Feature attribution,

MSW MANAGEMENT -Multidisciplinary, Scientific Work and Management Journal
ISSN: 1053-7899
Vol. 35 Issue 2, 2025, Pages: 597-630

confidence thresholding, and explainability integration ensure that classification decisions can be monitored and interpreted. These principles support intelligent diagnosis systems that operate with transparency and trust, especially in clinical environments [18]. Retinal image analysis benefits from such frameworks through enhanced visual reasoning and sample diversity, making the training process more resilient to noise, imbalance, and annotation gaps. Combining learning strategies with nature-inspired control mechanisms yields a more reliable and interpretable diagnostic outcome [19]. It introduces meaningful diversity and structured refinement in generative pathways.

1.1. Problem Statement

Diabetic retinopathy remains a leading cause of vision loss across the world, particularly among individuals with prolonged or unmanaged diabetes. Manual retinal screening through fundus photography is resource-intensive, time-consuming, and subject to variation across experts. Large-scale screening becomes impractical in low-resource settings, where trained ophthalmologists are limited. Existing automated classification models often depend on fully labelled datasets, struggle with inter-class overlap, and fail to generalize across demographic and clinical variations. Sample imbalance, feature ambiguity, and lack of transparency further degrade performance. These issues restrict the reliability and deployment of current image-based diagnostic tools in real-world healthcare systems.

1.2. Motivation

The growing burden of diabetes in both developed and developing regions has led to a sharp rise in vision-related complications, affecting working-age adults and elderly populations alike. Early detection of diabetic retinopathy provides an opportunity to prevent irreversible vision loss, maintain quality of life, and reduce treatment costs. Communities with limited access to ophthalmic care require diagnostic tools that are not only accurate but also adaptable and transparent. Enabling scalable, trustworthy image-based screening addresses a pressing healthcare gap. Optimizing learning systems to work under minimal supervision while preserving classification integrity can directly benefit vulnerable and underserved populations.

1.3. Objective

This research introduces a novel architecture, titled Dragonfly Swarm Optimized Semi-Supervised Generative Adversarial Network (DSO-SSGAN), for diabetic retinopathy classification using both labeled and unlabeled fundus images. The framework integrates biologically inspired dragonfly swarm behaviour into a semi-supervised adversarial learning environment to regulate latent sampling, enhance diversity, and stabilize class-wise representation. Confidence-based filtering, domain alignment, and interpretability components are incorporated to strengthen decision reliability. The objective is to ensure high diagnostic precision across severity stages, reduce dependence on annotated data, and address sample imbalance. DSO-SSGAN is designed for deployment in automated retinal screening pipelines serving diverse clinical and societal contexts.

2. LITERATURE REVIEW

"GAN-Enhanced Fundus Clarity" [20] is proposed for diabetic retinopathy detection by first enhancing fundus image quality using an EnlightenGAN, which clarifies key retinal details. The method then applies region-specific segmentation to highlight areas of concern. A transfer learning-based classifier processes these refined images to assign retinopathy stages, enabling timely identification through an integrated sequence of enhancement, segmentation, and classification with explicit image improvements.

MSW MANAGEMENT -Multidisciplinary, Scientific Work and Management Journal
ISSN: 1053-7899
Vol. 35 Issue 2, 2025, Pages: 597-630

"Graph-Driven Lesion Discovery" [21] is introduced as a technique that starts with pre-processing to remove non-disease regions from retinal images. Segmentation clusters then isolate retinal abnormalities using fuzzy techniques. A feature reduction phase enables efficient feature selection, followed by a Binary Chimp Algorithm to choose the most informative features possible. Finally, a Multi-Head Self-Attention Gated Graph Convolutional Network classifies retinopathy phases for robust diabetic retinopathy detection. "Sequential Visibility Amplification" [22] is designed as an approach that sequentially enhances the visibility of retinal haemorrhages in fundus scans through data augmentation and pre-processing. A compatible network, fine-tuned by transfer learning, further accentuates these structures for more effective classification. By combining visibility amplification with tailored model adaptation, the method enhances the visibility of disease features and maximizes the clarity of diabetic retinopathy identification from smaller clinical datasets.

"Hybrid Insightful Grader" [23] is implemented by merging a distributed convolutional feature extractor with a Light Gradient Boosting Machine. The convolutional step distils key traits from fundus and OCTA images, which LightGBM then classifies. Distributed learning not only reduces complexity but also delivers interpretable grade assignments, especially in cases where data imbalance and convergence issues have hampered past detection techniques for diabetic retinopathy. The "Branching Lesion Clarifier" [24] is designed by arranging a Swin-Transformer into multi-branch pipelines, allowing each branch to extract lesion features at distinct image scales in retinal images. Attention mechanisms highlight important regions, while cascading different feature streams enables fine separation of retinopathy grades. This careful structuring enhances the discrimination of diabetic retinopathy severity by focusing on disease-relevant parts. "Scale-Sensitive Lesion Fuser" [25] is developed to segment lesions of multiple sizes by merging dynamic attention-based feature hierarchies. The approach preserves image detail with Mobile Dynamic Attention Convolutions and combines semantic information across scales through a context fusion module. Such cascaded fusion ensures that both large and small lesions are separated precisely, leading to clear lesion boundaries that are crucial for further diagnosis stages.

The "Dual-View Focus Integrator" [26] is established to analyze fundus images using a dual-branch architecture; the transformer and convolutional streams process images in parallel. Lesion attention modules isolate relevant regions from each stream before fusing outputs, achieving synergy between local texture and broad context. This dual-focus mechanism amplifies the ability to grade and pinpoint diabetic retinopathy with accurate lesion understanding. The "Balanced CNN Feature Blender" [27] is formed by utilizing two customized networks to extract both local and global features from various stages of fundus imagery. The dataset is balanced using Synthetic Minority Oversampling, ensuring an adequate number of examples for rare classes. Feature sets from both networks are combined and delivered to multiple classifiers, providing nuanced diabetic retinopathy class distinction despite inherent data imbalance. The "Grade-Focused Style Filter" [28] is created by employing grade-aware channel similarity to minimize the grouping of images by acquisition domain rather than clinical grade. Grade-aware contrastive learning aligns cases of identical severity within feature space, and a multi-scale de-stylization step eliminates superficial style signals. The model thus remains focused on core lesion patterns, supporting consistent grading across many image sources.

The "Real-Time Multi-Scale Screener" [29] is constructed using a multi-scale feature extractor centred on layered filters that highlight various lesion types. All extracted features are compressed, then fed

MSW MANAGEMENT -Multidisciplinary, Scientific Work and Management Journal
ISSN: 1053-7899
Vol. 35 Issue 2, 2025, Pages: 597-630

into a streamlined classification stage. Paired with embedded hardware, the system enables efficient, real-time screening in clinics, supporting swift diabetic retinopathy grading through robust multi-scale feature analysis. "Hybrid Serial Ranker" [30] is designed as an ensemble that couples pre-trained feature extraction with recurrent classification layers. Spatial traits are captured using convolutional networks, while spatial relationships are processed through a recurrent pipeline. By layering these modules, the detector enables multi-stage retinopathy classification, reliably assigning retinopathy severity in complex presentation scenarios. The "Efficient Micro-Lesion Finder" [31] is proposed for the precise detection of very small, often-overlooked lesions within fundus images. The method employs feature pyramid and shallow network modules tailored to resource-limited settings. With a sharpened focus on minor abnormalities, the model annotates lesion locations for clinicians, ensuring that significant yet subtle disease signals are captured clearly. "Saliency-Guided Dual Refiner" [32] is introduced as a hierarchical dual-stage framework. In the initial phase, channel and spatial attention modules highlight lesion-rich retinal regions, and a second cross-attention phase refines these maps. The returned saliency information then guides the ultimate grading, making the entire process more transparent for medical professionals diagnosing diabetic retinopathy.

"Curvelet-SSO Optimization (C-SSO-O)" [33] proposes a framework that begins by reducing noise in retinal fundus images using a Wavelet Integrated Retinex algorithm. Following enhancement, Curvelet Convolutional Neural Networks (CCNN) analyze the images to classify diabetic retinopathy stages. The Salp Swarm Optimization (SSO) algorithm optimizes the CNN's activation functions, boosting classification accuracy and robustness. This integrated approach provides a refined, noise-reduced feature extraction with optimized learning dynamics, enhancing the detection of subtle diabetic retinopathy markers. "Inception-V4 DSLO Optimizer (I-V4-DSLO-O)" [34] introduces a deep learning method that integrates an optimized Inception-V4 architecture with a dynamic Snow Leopard Optimization (DSLO) algorithm. The DSLO fine-tunes feature selection to improve diabetic retinopathy detection from digital retinal images. This synergy enhances the model's sensitivity to early pathological signs like vessel leakage and edema, delivering improved classification accuracy and early-stage identification through adaptive optimization in complex retinal imagery.

MSW MANAGEMENT -Multidisciplinary, Scientific Work and Management Journal
ISSN: 1053-7899
Vol. 35 Issue 2, 2025, Pages: 597-630

Table 1. Technical and Qualitative Comparison of Diabetic Retinopathy Detection Methods

Nickname	Mechanism Description	Model Architecture	Feature Focus	Interpretability Level	Practical Advantage
GAN-Enhanced Fundus Clarity [20]	GAN-based quality enhancement enhances the clarity of raw images for deeper analysis through segmentation and CNN.	Transfer learning CNN	Enhanced retinal images	Moderate via ROI segmentation	Robust enhancement for low-quality images
Graph-Driven Lesion Discovery [21]	Uses graph convolution with optimized feature selection via evolutionary algorithm for precise lesion detection.	Gated Graph Convolutional Network	Abnormality segmentation	Moderate from feature analysis	Targets specific lesion features
Sequential Visibility Amplification [22]	Sequential data augmentation and preprocessing clarify haemorrhages, followed by tailored CNN classification.	Pre-trained CNN with fine-tuning	Hemorrhage-focused features	Low	Enhances the visibility of limited clinical datasets visibility
Hybrid Insightful Grader [23]	Combines distributed CNN features with a gradient boosting classifier for efficient multi-modal retinal image interpretation.	Distributed CNN + LightGBM	Fundus & OCTA fusion	High via explainability	Reduces complexity, improves accuracy
Branching Lesion Clarifier [24]	Multi-branch Transformer extracts lesion info at multiple scales using attention to distinguish severity fine-grainedly.	Swin-Transformer V2	Multi-scale lesion details	Moderate via attention maps	Fine-grained lesion feature retention
Scale-Sensitive Lesion Fuser [25]	Integrates multi-scale attention and dynamic convolution to segment both small and large lesions in fundus scans precisely.	U-Net with Mobile Dynamic Attention	Multi-scale lesion segmentation	Moderate with context fusion	Avoids semantic conflicts, precise segmentation
Dual-View Focus Integrator [26]	Parallel transformer and CNN branches extract complementary lesion features fused through attention for grading.	Dual-branch Transformer + CNN	Local and global lesion fusion	Moderate with saliency modules	Synergy across feature types aids grading
Balanced CNN Feature Blender [27]	Dual CNNs extract complementary features, while SMOTE addresses data imbalance, followed by the integration of multiple classifiers.	Custom ResNet50 and EfficientNet	Local and global spatial features	Low	Overcomes class imbalance robustly
Grade-Focused Style Filter [28]	Contrastive learning with de-stylization removes style bias, enforcing domain-invariant lesion-focused representations.	CNN with contrastive learning	Domain-invariant lesion features	Low to moderate	Improves cross-domain performance
Real-Time Multi-Scale Screener [29]	A multi-scale filter bank extracts nuanced lesion features that are compressible for real-time embedded system deployment.	Lightweight CNN	Multi-scale lesion features	Low	Efficient embedded screening
Hybrid Serial Ranker [30]	Combines CNN feature extraction with RNN spatial dependency modeling for sensitive spatial pattern classification.	CNN-RNN hybrid ensemble	Spatial + temporal DR features	Low	Captures spatio-temporal lesion relations
Efficient Micro-Lesion Finder [31]	A lightweight, improved detection architecture enhances the localization of small lesions using feature pyramids and layered attention.	Modified YOLOv5	Small lesion focus	Moderate through detection visualizations	Optimized for low-resource environments
Saliency-Guided Dual Refiner [32]	Hierarchical spatial and channel attention progressively refines lesion saliency for explainable grading decisions.	ResNet-18 with dual attention	Lesion saliency maps	High with saliency explanations	Enhances interpretability and grading accuracy
Curvelet-SSO Optimization [33]	Wavelet-filtered images pass through curvelet CNN with salp swarm optimization of activations for enhanced noisy feature extraction.	Curvelet CNN with SSO	Noise-reduced edge features	Moderate	Optimized learning with noise resilience
Inception-V4 DSLO Optimizer [34]	Inception-V4's deep layers refined via dynamic Snow Leopard Optimization improve adaptive feature selection for early retinal abnormalities.	Inception-V4 + DSLO	Early vascular/neural anomaly	Low	Enhanced early-stage detection

MSW MANAGEMENT -Multidisciplinary, Scientific Work and Management Journal
ISSN: 1053-7899
Vol. 35 Issue 2, 2025, Pages: 597-630

3. DRAGONFLY SWARM OPTIMIZED SEMI-SUPERVISED GENERATIVE ADVERSARIAL NETWORK

The proposed framework, Dragonfly Swarm Optimised Semi-Supervised GAN (DSO-SSGAN), is designed to address the complexities in retinal image classification, particularly in detecting the severity of diabetic retinopathy. Inspired by the intelligent swarm coordination of dragonflies during foraging, the system combines biologically motivated search dynamics with semi-supervised adversarial learning. By integrating swarm-based optimization into latent sampling and embedding interpretability throughout the pipeline, the model ensures both performance and trustworthiness. This architecture enables the effective utilization of both labelled and unlabeled data, enforces output diversity, adapts to unseen domains, and facilitates transparent decision-making through generator attribution analysis.

3.1. Dataset Preparation with Class Imbalance Aware Encoding

The initiation of the DSO-SSGAN pipeline begins with a crucial preprocessing stage, specifically, dataset preparation, which explicitly addresses class imbalance. In diabetic retinopathy (DR) classification, the early, moderate, and severe stages are unequally represented in real-world data, necessitating bio-inspired optimization in encoding strategies. Reflecting the exploratory food-searching phase of a dragonfly swarm, this step ensures that labelled samples are not only uniformly acknowledged but also semantically structured to support class-conditional generation and discrimination in the later adversarial and optimization stages.

A labelled dataset $D = \{(x_i, y_i)\}_{i=1}^{N}$, where $x_i$denotes retinal fundus images and $y_i \in \{1,2,\ldots,K\}$ represents DR severity classes partitioned based on frequency distribution per class. Let n_k be the number of samples in class k, then the class weight w_k is defined by Eq.(1).

$$w_k = \frac{1}{log(\delta + n_k)} \quad (1)$$

where δ is a smoothing constant preventing undefined weights for rare classes. This logarithmic scaling mimics the dragonfly's diminishing sensitivity to redundant stimuli in dense environments, thus favouring exploration towards under-represented classes during optimization.

To align with swarm-based discrimination, class labels are encoded into dense, optimizable class vectors $y_k \in R^d$, ensuring semantic conditioning. The encoding process adheres to an energy-minimizing transformation:

$$y_k = \arg\min_{v_k} \sum_{j \neq k} \frac{1}{\|v_k - v_j\|^2 + \epsilon} \quad (2)$$

Eq.(2) imitates the repulsion-separation phase in dragonfly swarms, where vectors seek discriminative separability while maintaining minimal overlaps, which is crucial in distinguishing subtle DR severity gradients. The initial sampling for training the generator and discriminator is probabilistically rebalanced using a normalized selection matrix $P \in R^K$:

$$P_k = \frac{w_k}{\sum_{j=1}^{K} w_j} \quad (3)$$

Eq. (3) guides the first iteration of memory formation, akin to the swarm's memory-influenced directional choice, enabling the model to revisit hard-to-classify samples from rare DR stages frequently. This selection matrix ensures that generator inputs across swarm iterations reflect class diversity.

To condition the generator, latent noise $z \sim N(0,1)$ is fused with class embeddings via a bilinear fusion operator:

$$h_i = \phi(z_i, y_i) = z_i \odot tanh(W \cdot y_i + b) \quad (4)$$

MSW MANAGEMENT -Multidisciplinary, Scientific Work and Management Journal
ISSN: 1053-7899
Vol. 35 Issue 2, 2025, Pages: 597-630

In Eq.(4), $W \in R^{d\times d}$ and $b \in R^{d}$ are learnable parameters. The Hadamard product $\odot$ introduces non-linear interdependence, enhancing class-specific generation behaviour and modelling dragonfly attraction to class-conditioned 'food' vectors within the feature swarm space.

The spatial embedding of samples in the input space follows a topology-preserving distribution, mimicking a swarm-like positioning. Each class centroid μ_k in feature space is defined as Eq.(5) and the feature map $f(x_i)$ is extracted via a pretrained backbone. These centroids guide the positioning of newly sampled points, allowing subsequent steps (like DSO sampling) to align their vectors with centroids via attraction-influenced paths, representing food-seeking vector fields in a DR-class manifold.

$\mu_k = \frac{1}{n_k}\sum_{i:y_i=k} f(x_i)$	(5)

In adherence to a progressive learning philosophy, samples are dynamically scheduled from simple to complex using an entropy-based difficulty score:

$Difficulty(x_i) = -\sum_{k=1}^{K} p_k(x_i) log p_k(x_i)$	(6)

In Eq.(6), $p_k(x_i)$ is the predicted softmax probability from a warm-start classifier. The entropy mirrors perception alignment in dragonfly decision latency—lower entropy samples are introduced early, and complex (high-entropy) samples are gradually incorporated as the model gains confidence in feature separability.

3.2. Dragonfly Swarm Initialization with Adaptive Dynamics

Following the class-balanced encoding stage, the swarm initialization phase activates the computational analogy of dragonfly foraging. Dragonflies form dynamic spatial groups while hunting, guided by principles of alignment, cohesion, separation, and external stimuli. In the DSO-SSGAN pipeline, each virtual dragonfly represents either a latent generator input or a learned feature transformation. This step generates an adaptive swarm whose flight vectors navigate the latent space landscape, targeting class-specific feature zones within the image manifold of diabetic retinopathy severity levels.

Each dragonfly in the population is encoded as a vector $d_i \in R^m$, where $m = d_z + d_y$, combining latent vector length and class embedding. The initial position of the i^{th}dragonfly is:

$d_i^0 = \gamma z_i + (1-\gamma)\cdot y_i$	(7)

In Eq.(7), $z_i \sim N(0, \sigma^2 I)$ and y_i is a class vector from Step 1. The scalar $\gamma \in [0,1]$ modulates the dominance of random vs. class-conditioned exploration, reflecting swarm sensitivity to environmental bias during early foraging.

Each dragonfly is assigned an initial velocity vector v_i^0oriented towards the class centroid μ_{y_i} in feature space. The velocity is computed as:

$v_i^0 = \eta \cdot \frac{\mu_{y_i} - G(d_i^0)}{\left\|\mu_{y_i} - G(d_i^0)\right\| + \epsilon}$	(8)

Where $G(\cdot)$ denotes the generator output and η is a learning constant. This velocity initialization mimics attraction-based movement toward promising regions of high image similarity, a hallmark of dragonfly predation.

MSW MANAGEMENT -Multidisciplinary, Scientific Work and Management Journal
ISSN: 1053-7899
Vol. 35 Issue 2, 2025, Pages: 597-630

To regulate motion damping, an inertia factor ω_t is dynamically updated per iteration t as:

$$\omega_t = \omega_{max} - \left(\frac{\omega_{max} - \omega_{min}}{T}\right) \cdot t \quad (9)$$

In Eq.(9), ω_{max} and ω_{min} are the upper and lower inertia bounds, and T is the total number of iterations. This temporal decay induces a transition from aggressive exploration to stable convergence, paralleling the dragonfly's shift from global search to target fixation. To encourage balanced spacing among swarm members, initial separation S_i^0 and cohesion C_i^0 vectors for each dragonfly are calculated as Eq.(10) and Eq.(11)

$$S_i^0 = \frac{1}{N}\sum_{j \neq i} \frac{d_i^0 - d_j^0}{\left\|d_i^0 - d_j^0\right\|^2 + \epsilon} \quad (10)$$

$$C_i^0 = \frac{1}{N}\sum_{j \neq i} d_j^0 - d_i^0 \quad (11)$$

These components replicate the collision avoidance and center-seeking tendencies observed in collective motion systems and are essential for retaining swarm coherence across iterations. Each dragonfly also aligns with its velocity-matching neighbours. The alignment vector A_i^0 is defined as Eq.(12).

$$A_i^0 = \frac{1}{N}\sum_{j \neq i} \left(v_j^0 - v_i^0\right) \quad (12)$$

Alignment ensures that swarm members follow a consensus trajectory, resembling the dragonfly's synchronous hovering and navigation, which is beneficial for robust DR class boundary approximation in latent space.

To guide swarm evolution, "food" and "enemy" vectors are assigned based on elite performance (i.e., the best-generated samples) and poor fitness (i.e., the worst misclassifications). The respective attraction/repulsion vectors are:

$$F_i^0 = \theta_1 \cdot \frac{d_{food} - d_i^0}{\left\|d_{food} - d_i^0\right\| + \epsilon} \quad (13)$$

$$E_i^0 = \theta_2 \cdot \frac{d_{enemy} - d_i^0}{\left\|d_{enemy} - d_i^0\right\| + \epsilon} \quad (14)$$

The scalar weights θ_1 and θ_2 denote the attraction to best solutions and repulsion from error zones, respectively, simulating predator-prey sensitivity in dragonfly swarms.

The final initialized velocity vector V_i^0 for each dragonfly, the combined swarm forces with inertia are mathematically expressed as Eq. (15).

$$V_i^0 = \omega_t \cdot v_i^0 + sS_i^0 + aA_i^0 + cC_i^0 + fF_i^0 - eE_i^0 \quad (15)$$

The coefficients s, a, c, f, e are behaviour constants for separation, alignment, cohesion, food attraction, and enemy avoidance. This formulation enables each swarm agent to explore class-encoded image generation zones optimized for DR prediction tasks.

MSW MANAGEMENT -Multidisciplinary, Scientific Work and Management Journal
ISSN: 1053-7899
Vol. 35 Issue 2, 2025, Pages: 597-630

3.3. Multi-Objective Fitness Function Evaluation

Once the dragonfly swarm has been initialized with class-specific vectors and adaptive motion states, the next critical operation involves computing a composite fitness score. This score determines each dragonfly's survival, reproduction, and role in guiding the swarm toward optimal generator input. Much like dragonflies dynamically assess prey potential based on motion cues and visual saliency, this fitness evaluation blends classification, adversarial deception, feature similarity, and diversity metrics. Each generated image is scored not on a single utility but across a harmonized multi-objective surface.

Each generated image $\hat{x}_i = G(d_i)$, produced by the generator using the position vector of a dragonfly, is passed to the discriminator ensemble. The logit-aligned confidence defines the classification alignment score:

$$F_i^{(1)} = log\left(1 + \sigma_k(\hat{x}_i)\right) \quad (16)$$

In Eq.(16), $\sigma_k(\hat{x}_i)$ is the softmax activation corresponding to the true class k predicted by the discriminator. The logarithmic transformation ensures gradient stability while mimicking the dragonfly's sharpened targeting precision when confidence in the prey class is high.

To preserve the generative adversarial nature of the SS-GAN structure, an adversarial fitness term evaluates the likelihood that the generated image is mistaken as real by the discriminator. The adversarial deception component is modeled as Eq. (17).

$$F_i^{(2)} = \left(\frac{1}{1 + e^{-L_D(\hat{x}_i)}}\right) \quad (17)$$

In Eq.(17), $L_D(\hat{x}_i)$ is the discriminator's real/fake binary logit before softmax activation. A higher deception score mirrors the dragonfly's ability to camouflage intent and penetrate target zones undetected.

To ensure that the generated image not only tricks the discriminator but also semantically resembles the class it represents, a perceptual loss is introduced. The perceptual similarity fitness is defined using a deep feature extractor Ψ:

$$F_i^{(3)} = exp(-\|\Psi(\hat{x}_i) - \Psi(\mu_k)\|^2) \quad (18)$$

In Eq.(18), μ_k represents the class centroid in the feature domain. The exponential scaling rewards proximity, much like dragonflies fine-tune their attack angles based on motion blur reduction and visual cue consistency. To prevent the generator from producing similar samples across the swarm (mode collapse), a swarm-level diversity score is embedded. This term is calculated for each dragonfly against the current elite members:

$$F_i^{(4)} = \sum_{j=1}^{M}\left(1 - \frac{\hat{x}_i \cdot \hat{x}_j}{\|\hat{x}_i\| \cdot \|\hat{x}_j\|}\right) \quad (19)$$

MSW MANAGEMENT -Multidisciplinary, Scientific Work and Management Journal
ISSN: 1053-7899
Vol. 35 Issue 2, 2025, Pages: 597-630

In Eq. (19), the dot product represents the cosine similarity between the generated samples. A higher score promotes dissimilarity, reflecting the dragonfly's tendency to spread out when exploring territory with competitive prey density. The latent vector and class label fused at the generator input must yield output images that are consistent with the class semantics. This alignment is captured through the latent-class consistency score:

$$F_i^{(5)} = \frac{1}{1 + \left\| z_i - F^{-1}(G(d_i)) \right\|} \quad (20)$$

In Eq.(20), $F^{-1}(\cdot)$ is an inverse projection or approximation of the latent embedding recovered from the generated image. The scoring encourages the generation of class-faithful images, simulating how dragonflies prioritize recall cues from prior foraging cycles. Each class exists within a latent decision boundary learned by the discriminator. A margin-based score is introduced to reward samples that fall within high-certainty class zones but not near inter-class boundaries:

$$F_i^{(6)} = \max_{m \neq k} (\sigma_k(\hat{x}_i) - \sigma_m(\hat{x}_i)) \quad (21)$$

Eq.(21) ensures separation between class predictions. The margin sharpness replicates the dragonfly's enhanced ability to discriminate between optimal prey and a noisy environment. The final composite score F_i for each dragonfly is a weighted summation of all the sub-objectives:

$$F_i = \lambda_1 F_i^{(1)} + \lambda_2 F_i^{(2)} \lambda_3 F_i^{(3)} \lambda_4 F_i^{(4)} \lambda_5 F_i^{(5)} \lambda_6 F_i^{(6)} \quad (22)$$

In Eq.(22), λ_j represents a tunable hyperparameter that governs the influence of each behavioural term. These coefficients form the fitness landscape that defines the dynamic reorientation of the swarm for subsequent positional updates. This is analogous to how dragonflies prioritize prey proximity, size, movement, and velocity fields when engaging in collective attack formations.

3.4. Latent Space Regularization

Latent space regularization ensures that the dragonfly swarm navigates a generative domain where image transitions reflect real-world disease progression. Within DSO-SSGAN, each dragonfly's latent position must yield a perceptually plausible and class-consistent sample. Similar to dragonflies maintaining minimal-energy trajectories across fluid terrains, the latent space must exhibit smooth continuity, structural cohesion, and clear class boundary margins. This regularization stage limits abrupt generator output shifts and embeds meaningful topology into the search domain for accurate diabetic retinopathy classification.

To maintain continuity across neighbouring latent vectors, a pairwise smoothness penalty is introduced. Given two nearby latent samples $z_i$and z_j, the regularization term is defined as:

$$R_1 = \frac{1}{\left\| z_i - z_j \right\|^2 + \epsilon} \cdot \left\| G(z_i, y_i) - G(z_j, y_j) \right\|^2 \quad (23)$$

In Eq.(23), $G(z, y)$ represents the generator output conditioned on class embedding y. The regularization discourages minor latent differences from producing disproportionate output variations, imitating how dragonflies maintain wing stability under small angular perturbations.

MSW MANAGEMENT -Multidisciplinary, Scientific Work and Management Journal
ISSN: 1053-7899
Vol. 35 Issue 2, 2025, Pages: 597-630

To prevent volatile changes in generated features across swarm movement, a directional gradient norm is controlled. For a latent direction vector u_i, define:

$$R_2 = \left\| \frac{\partial G(z_i + \delta u_i y_i)}{\partial \delta} \right\|^2 \quad (24)$$

This constraint ensures that the change in generator output with respect to latent motion remains bounded. Dragonflies adjust flight strength incrementally during angular redirection—a similar principle is enforced here within latent perturbation corridors. Swarm dragonflies associated with a particular class must reside near the corresponding class manifold. Define the class-centroid proximity regularization as Eq.(25):

$$R_3 = \left\| z_i - \bar{z}_{y_i} \right\|^2 \quad (25)$$

Where $\bar{z}_{y_i}$ is the centroid of all latent vectors producing the class y_i. This penalization aligns swarm agents with their class-focused cluster centre, replicating dragonfly convergence on a nutritional target source when searching collectively.

To maintain high inter-class separability, latent vectors are pushed away from decision boundaries. For class labels $y_i \neq y_j$, a margin regularization is defined as Eq. (26). It enhances the structural margin between different class manifolds, emulating how dragonflies maintain safe distances between rival flocks to avoid entanglement and resource conflict.

$$R_4 = \frac{1}{\left\| z_i - z_j \right\|^2 + k} \quad (26)$$

To improve global latent coherence, all vectors are penalized based on their deviation from the swarm's centre of gravity in latent space:

$$R_5 = \frac{1}{N} \sum_{i=1}^{N} \| z_i - \mu_z \|^2 \quad (27)$$

In Eq.(27), $\mu_z = \frac{1}{N} \sum_{i=1}^{N} z_i$ is the latent centroid. This term compacts the swarm into a navigable structure, promoting group cohesion like how dragonfly swarms exhibit geometric tightness under central guidance.

To maintain the invertibility of the generator's transformation, the latent vector is regularized through a learned decoder D^{-1} that approximates the latent encoding from generated outputs:

$$R_6 = \left\| z_i - D^{-1}\left(G(z_i, y_i)\right) \right\|^2 \quad (28)$$

This regularization facilitates bi-directional mappings, ensuring that latent positions have meaningful representations in image space. In a behavioural parallel, dragonflies exhibit positional recall, retracing paths via memory-informed loops—this constraint encodes that memory retention effect computationally.

3.5. Diversity Preservation Constraint

As swarm movement progresses, preventing collapse into narrow or repetitive regions becomes critical for meaningful exploration. Inspired by the widespread scattering of dragonflies when competing over dense prey regions, this step embeds diversity enforcement directly into the generative process. Within the DSO-SSGAN context for diabetic retinopathy classification, class-consistent yet visually diverse images are essential to reflect pathological variance. This constraint introduces inter-sample dissimilarity and intra-class spread to maintain the swarm's exploratory richness and prevent image redundancy in the generated datasets for diabetic images.

MSW MANAGEMENT -Multidisciplinary, Scientific Work and Management Journal
ISSN: 1053-7899
Vol. 35 Issue 2, 2025, Pages: 597-630

Each generated sample $\hat{x}_i = G(z_i, y_i)$ is evaluated against other generator outputs using a cosine-based dissimilarity function:

$$D_1 = \sum_{i=1}^{N} \sum_{j \neq i} \left(1 - \frac{\hat{x}_i \cdot \hat{x}_j}{\|\hat{x}_i\| \cdot \|\hat{x}_j\| + \epsilon}\right) \quad (29)$$

In Eq.(29), the numerator represents the dot product of image tensors, and the denominator is a product of their Euclidean norms. This metric penalizes angular similarity between feature vectors, promoting diverse orientations akin to the way dragonflies alter their flight angles to prevent mid-air interference during collective foraging.

Generated samples sharing the same class label must display structural variety while remaining semantically coherent. A class-level diversity constraint is formulated as shown in Eq. (30).

$$D_2 = \sum_{k=1}^{K} \frac{1}{n_k^2} \left\|\phi(\hat{x}_i) - \phi(\hat{x}_j)\right\|^2 \quad (30)$$

where, C_k denotes the set of generated samples from class k, and $\phi(\cdot)$ is a pre-trained feature extractor mapping images to perceptual space. This constraint ensures that generator outputs within the same class distribution avoid redundancy, emulating the dynamic inter-dragonfly distance when multiple agents pursue prey from similar directions.

To preserve richness at the distributional level, a feature covariance-based dispersion is introduced. Given feature activations $f_i = \phi(\hat{x}_i)$, the global covariance matrix is represented as Eq.(31) and The diversity loss is then defined as Eq.(32).

$$E_f = \frac{1}{N} \sum_{i=1}^{N} (f_i - \bar{f})(f_i - \bar{f})^T \quad (31)$$

$$D_3 = -Tr(\Sigma_f) \quad (32)$$

where $\bar{f}$ is the mean activation vector and $Tr(\cdot)$ denotes the matrix trace. Maximizing the trace of the covariance matrix encourages feature dimensions to decorate, just as dragonflies avoid synchronized motion to maximize coverage.

In addition to the trace, the determinant of the covariance matrix is also used to assess volumetric spread in the feature space:

$$D_4 = -\log(det(\Sigma_f) + \delta) \quad (33)$$

where δ is a stabilizing term to prevent logarithmic singularity, the determinant reflects the occupied hypervolume of feature distributions and increases when the generated samples span orthogonal perceptual directions—mirroring spatial breadth in swarm formations.

Entropy from singular value decomposition of the Gram matrix of feature vectors $F = [f_1, f_2, .., f_N]$ is used to capture generator variability:

MSW MANAGEMENT -Multidisciplinary, Scientific Work and Management Journal
ISSN: 1053-7899
Vol. 35 Issue 2, 2025, Pages: 597-630

$D_5 = -\sum_{i=1}^{r} \lambda_i log(\lambda_i + \delta)$	(34)

In Eq.(34), λ_i are the normalized singular values of $F^T F$, and r is the rank. Higher entropy corresponds to a balanced usage of feature dimensions, mapping directly to dragonfly swarms that utilize multi-sensor coordination for adaptive hovering and pursuit.

To improve latent-to-output disentanglement, pairwise mutual dependence between generated samples is penalized using kernel-based independence:

$D_6 = \sum_{i=1}^{N} \sum_{j \neq i} k(\hat{x}_i, \hat{x}_j)$	(35)

In Eq.(35), $k(\cdot,\cdot)$ is a positive semi-definite kernel function, such as Gaussian RBF. A higher aggregate kernel sum indicates redundancy, while minimization encourages independence, emulating how dragonflies utilize non-overlapping visual regions to reduce sensory redundancy.

To indirectly enforce output variation, spacing in the latent domain is encouraged using a latent spread term, as expressed in Eq. (36), which discourages the clustering of latent vectors in tight zones, thereby promoting broad coverage of the generative space. In natural foraging, dragonflies reposition in wider loops around prey sites to cover a greater sensory volume—this constraint replicates their spatial repositioning behavior.

$D_7 = \sum_{i=1}^{N} \sum_{j \neq i} \frac{1}{(z_i - z_j)^2 + \epsilon}$	(36)

All eight diversity-promoting terms are combined into a unified loss function with tunable scalar weights β_t:

$D_{total} = \sum_{l=1}^{7} \beta_l D_l$	(37)

Each β_l allows specific control over the influence of diversity elements, which can be modulated during swarm evolution stages. The total constraint maintains variety in both visual content and structural semantics of generated images, ensuring that the DR classification framework learns from rich, non-redundant training signals akin to a dragonfly's exposure to variable prey patterns.

3.6. Dragonfly Behavioural Update with Elitism and Class-Aware Swarm Partitioning

Following fitness evaluation and diversity enforcement, swarm behavioural adjustments are executed to regulate the latent search process. Dragonflies exhibit layered swarm roles, with a subset acting as elite leaders guiding spatial adaptation. Similarly, in DSO-SSGAN, swarm updates incorporate behavioural vectors informed by local alignment, inter-class awareness, and centroid tracking. The diabetic retinopathy classification context benefits from class-wise swarm structuring, as disease stages require precise separation. This phase realigns swarm dynamics based on individual and class-oriented objectives to optimize image generation diversity and diagnostic relevance.

MSW MANAGEMENT -Multidisciplinary, Scientific Work and Management Journal
ISSN: 1053-7899
Vol. 35 Issue 2, 2025, Pages: 597-630

Each dragonfly's latent-class position vector $d_i^{t+1}$is modified based on behavioural velocities accumulated from various forces at iteration t. The position update is defined as Eq.(38), and in that ρ is a dynamic scaling factor controlling exploration depth and V_i^t is the aggregated behavioural velocity. This update maintains consistent flight momentum, similar to the inertial motion exhibited by dragonflies as they adapt their trajectories in swarms.

$$d_i^{t+1} = d_i^t + \rho \cdot V_i^t \quad (38)$$

The composite velocity V_i^t aggregates multiple behavioural components: alignment, cohesion, separation, class-centroid attraction, and noise avoidance. The update rule is represented as Eq.(39), and each term corresponds to: A_i^t (alignment), C_i^t (cohesion), S_i^t (separation), Q_i^t (class-centroid force), and N_i^t (nearest misclassified sample repulsion). Scalars $\alpha, \beta, \gamma, \lambda, \theta$ govern directional dominance. The coordination closely models dragonfly field formations, where group compliance and error avoidance dictate locomotion.

$$V_i^t = \alpha A_i^t + \beta C_i^t + \gamma S_i^t + \lambda Q_i^t - \theta N_i^t \quad (39)$$

Swarm elitism ensures that top-performing agents have a positive influence on future generations without compromising their integrity. Define the elite subset ε^t using Eq.(40) and F_i^t is the fitness of dragonfly i, and δ is the elite threshold margin. Elite retention fosters convergence stability while guiding exploration, similar to how dominant dragonflies lead coordinated attacks near prey hotspots.

$$\varepsilon^t = \{d_i^t | F_i^t \geq max(F^t) - \delta\} \quad (40)$$

To retain inter-class separation and intra-class cohesiveness, swarm members are grouped by class label. Let Eq.(41) be the class-specific subset S_k^t and each subset evolves independently, allowing class-specific trajectory dynamics. This formulation supports more precise classification boundaries, emulating how dragonflies distribute by task roles during multipoint predatory episodes.

$$S_k^t = \{d_i^t | y_i = k\} \quad (41)$$

Each swarm cluster aligns with its local class-centric reference point $\bar{d}_k^t$, calculated as Eq.(42) and the cohesion term C_i^t is then redefined to attract each member of S_k^t towards its local centroid. This mirrors the internal looping migration of dragonflies around dominant leaders in a class-coded hierarchy of attention.

$$\bar{d}_k^t = \frac{1}{|S_k^t|} \sum_{d_j \in S_k^t} d_j^t \quad (42)$$

To avoid convergence towards misclassified zones, swarm members are repelled from recently failed latent vectors M^t, computed via Eq.(43), and the behavioural response reduces the tendency to revisit error-prone image generators, mimicking the avoidance of predator-disturbed zones in natural swarm dispersal.

$$N_i^t = \sum_{d_m \in M^t} \frac{d_i^t - d_m}{\|d_i^t - d_m\|^2 + \epsilon} \quad (43)$$

MSW MANAGEMENT -Multidisciplinary, Scientific Work and Management Journal
ISSN: 1053-7899
Vol. 35 Issue 2, 2025, Pages: 597-630

Scalars $\alpha, \beta, \gamma, \lambda, \theta$ in the velocity update are dynamically adjusted based on the fitness variance within the swarm. Let Eq.(44) be the fitness standard deviation. σ_F^t, where the coefficients follow similar transformations. A tighter swarm leads to a smaller. σ_F^t, triggering increased repulsion and reduced alignment, enhancing divergence akin to defensive realignments in a dragonfly's threat-sensitive clustering.

$\alpha = \frac{1}{1 + e^{-\sigma_F^t}}, \ \theta = 1 - \alpha$	(44)

3.7. Generator Training - DSO + Gradient + Curriculum Strategy

Training the generator within DSO-SSGAN integrates a dual mechanism inspired by the decision-making of a foraging dragonfly. This hybrid system blends dragonfly swarm optimization and gradient-based fine-tuning, supported by a progressive curriculum scheduler. The goal is to refine class-specific retinal image generation for the detection of diabetic retinopathy. Dragonflies alternate between instinct-driven exploration and precision-controlled pursuit, a behaviour that is algorithmically reflected in the combination of discrete swarm movement and local gradient descent employed in this generative learning stage.

The generator's loss function combines terms for adversarial, perceptual, class consistency, and structural diversity. This composite formulation is defined as Eq.(45) and $\eta_1, \eta_2, \eta_3, \eta_4$ are tunable scalar coefficients. The multi-objective formulation allows the generator to synthesize diabetic fundus images that are not only realistic but also semantically aligned and perceptually rich, resembling the multiple targeting signals perceived by a dragonfly in prey selection.

$L_G = \eta_1 L_{adv} + \eta_2 L_{cls} + \eta_3 L_{perc} + \eta_4 L_{div}$	(45)

The generator receives latent-class input vectors selected by the dragonfly swarm. Each position update from Swarm Evolution provides a candidate input:

$z_i^* = d_i^{t+1}$	(46)

In Eq.(46), d_i^{t+1} is the final position after behaviour-based swarm movement. The generator synthesizes $G(z_i^*)$, and the result is evaluated using multi-objective loss. The optimized generation process reflects the dragonfly's looped decision path from position updates to target focus.

After swarm-guided latent selection, generator weights are updated using gradient descent with respect to the multi-branch loss. Let θ_G be the generator parameters in Eq.(47). η is the learning rate, the gradient term aggregate was adversarial, class-matching, and perceptual feedback. This mimics how dragonflies adapt wing force post navigation, recalibrating acceleration for improved focus and tracking.

$\theta_G \leftarrow \theta_G - \eta \cdot \nabla_{\theta_G} L_G$	(47)

The adversarial component is defined through the discriminator's output over generated images, and Eq. (48) increases the generator's ability to mislead the discriminator into misclassifying fake images as real. It enforces plausible DR image generation, reproducing retinal tissue characteristics crucial for stage classification.

MSW MANAGEMENT -Multidisciplinary, Scientific Work and Management Journal
ISSN: 1053-7899
Vol. 35 Issue 2, 2025, Pages: 597-630

$L_{adv} = -E_{z\sim p_z(z)}[log(D(G(z,y)))]$	(48)

To ensure the generated image aligns with the conditional class label, a categorical loss is calculated as shown in Eq. (49).

$L_{cls} = -\sum_{k=1}^{K} y_k \cdot log(D_k(G(x,y)))$	(49)

In Eq.(49), D_k is the discriminator's prediction for class k, and y_k is the one-hot encoded accurate to label. This enforces class-specific detail preservation, comparable to the visual salience dragonflies maintain while trailing specific prey patterns. Training samples are scheduled progressively based on difficulty. Let S_τ be the sample subset at curriculum level τ, defined using an entropy metric:

$S_\tau = \{x_i \mid H(D(G(z_i))) < \delta_\tau\}$	(50)

In Eq.(50), $H(\cdot)$ is entropy and δ_τ is a difficulty threshold. The curriculum strategy simulates how dragonflies gradually hone in on high-speed prey after mastering the predictable movement. The perceptual fidelity of generated images is captured using a deep feature comparator $\Phi(\cdot)$:

$L_{perc} = \left\|\Phi\left(G(z,y)\right) - \Phi(x_{real})\right\|^2$	(51)

In Eq.(51), x_{real} is a sample from the ground truth class. This term ensures structural similarity in deep space, similar to the dragonfly's alignment of current visual signals with memory-referenced patterns. Generator updates incorporate a diversity penalty between mini-batch outputs, as expressed in Eq. (52), which discourages redundancy. Dragonflies flying in formation instinctively spread out across sensory volumes; this loss encodes such instinctive dispersal within the generative process.

$L_{div} = \sum_{i=1}^{n}\sum_{j>i}^{n}\left(\frac{1}{\left\|G(z_i,y_i) - G(z_j,y_j)\right\|^2 + \epsilon}\right)$	(52)

3.8. Supervised Discriminator Training with Ensemble and Explainability

Swarm convergence towards meaningful latent directions relies on consistent guidance from a discriminator that simultaneously recognizes semantic class structures and enforces authenticity. This step incorporates a supervised ensemble of discriminators, allowing multi-perspective analysis of generator outputs across class partitions. Each member operates independently, enhancing robustness in classification and adversarial discrimination. Inspired by dragonfly groups assessing a target from multiple angles, this framework embeds redundancy-aware accuracy into diabetic retinopathy prediction. In addition to ensemble consensus, explainability maps, such as Grad-CAM, are integrated into the learning loop, visually reinforcing feature focus and contributing to medically interpretable fundus image classification.

Each discriminator D_m, indexed by $m \in \{1,2,\ldots,M\}$, classifies authentic and generated images across K diabetic retinopathy categories. The softmax prediction vector is defined as Eq.(53) and $f_m(x)$ denotes the feature map extracted by the m^{th} discriminator for input x, with trainable weights W_m and

MSW MANAGEMENT -Multidisciplinary, Scientific Work and Management Journal
ISSN: 1053-7899
Vol. 35 Issue 2, 2025, Pages: 597-630

biases b_m. This transformation estimates class-wise probabilities, similar to how dragonfly units allocate attention weights across directional sectors when tracking dynamic targets in prey-dense regions.

$$\hat{y}_m(x) = Softmax(W_m f_m(x) + b_m) \quad (53)$$

The categorical cross-entropy loss is computed over the actual label vector $y \in R^K$ and predicted output $\hat{y}_m(x)$ as Eq. (54), it penalizes misclassification proportionally to confidence, helping the discriminator assign stage-specific diagnostic tags across different DR types. The sharpness of the penalty correlates with class deviation distance, replicating swarm realignment when a scout misidentifies a visual trace.

$$L_{sup}^{(m)} = -\sum_{k=1}^{K} y_k \cdot log\left(\hat{y}_{m,k}(x)\right) \quad (54)$$

Discriminators also perform binary classification of image authenticity. For an image x, whether real or generated, the authenticity prediction is expressed as Eq.(55).

$$\hat{a}_m(x) = \sigma(U_m^T f_m(x) + c_m) \quad (55)$$

Where, σ denotes the sigmoid function, and U_m, c_m are parameters of the binary decision layer for the m^{th} ensemble member. This component replicates the dragonfly's dual process, first detecting a potential target and then verifying the authenticity of the prey before pursuit.

Adversarial loss for the discriminator D_m is calculated as Eq.(56).

$$L_{adv}^{(m)} = \left[a \cdot log\left(\hat{a}_m(x)\right) + (1-a) \cdot log\left(1 - \hat{a}_m(x)\right)\right] \quad (56)$$

Where $a = 1$ for authentic images and $a = 0$ for generated ones. This binary divergence aligns swarm judgment on authenticity verification with retinal image realism, echoing the mechanism of pursuit rejection during the recognition of deceptive visual signals.

The overall supervised discriminator loss per ensemble member is weighted as shown in Eq. (57).

$$L_{D_m} = \alpha_1 \cdot L_{sup}^{(m)} + \alpha_2 \cdot L_{adv}^{(m)} \quad (57)$$

Where α_1, α_2 balance the influence of classification and adversarial learning. These scalar controls reflect the swarm's dual-channel decision-making process: one path for categorization, the other for authenticating the target.

Ensemble training consolidates all members' feedback into a single, comprehensive view. Eq.(58) expresses the collective discriminator loss. This averaging enables robustness against noisy members, offering a fault-tolerant backbone to guide generator evolution. The approach replicates swarm-wide averaging in environmental navigation, where movement consensus emerges from the spatial aggregation of signals.

$$L_D = \frac{1}{M}\sum_{m=1}^{M} L_{D_m} \quad (58)$$

MSW MANAGEMENT -Multidisciplinary, Scientific Work and Management Journal
ISSN: 1053-7899
Vol. 35 Issue 2, 2025, Pages: 597-630

Parameter updates for each discriminator D_m follow gradient descent using Eq.(59).

$\theta_{D_m} \leftarrow \theta_{D_m} - \eta_d \cdot \nabla_{\theta_{D_m}} L_{D_m}$	(59)

Where, η_d is the learning rate. Updates rely on a total loss, involving both class and authenticity cues. This mirrors the neuromuscular refinement in dragonfly locomotion, where signal convergence readjusts wing-torque execution to stabilize positioning in wind-disrupted flight corridors.

Explainability maps $M_m(x)$are extracted using Grad-CAM from the final convolutional feature map $F_m$and gradients $g_m^k = \partial_{\hat{y}_{m,k}}/\partial F_m$ as Eq.(60).

$M_m(x) = ReLU\left(\sum_c \omega_{m,c} F_m^{(c)}\right)$	(60)

Where $\omega_{m,c} = \frac{1}{Z}\sum_{i,j} g_{m,c'}^{i,j}$ and Z is the spatial dimension of F_m. These maps highlight image regions most influential in classification, simulating visual locking in dragonflies, which stabilize their heads by locking onto edge contrasts for prey capture.

To ensure consistency in Grad-CAM focus maps across training iterations, a divergence loss between consecutive maps is defined as in Eq. (61). This additional constraint improves model interpretability by maintaining a stable class-sensitive focus over time. The reliability of swarm orientation mirrors this strategy, where revisiting familiar terrain yields reinforced neural mapping in the dragonfly's trajectory recall.

$L_{cam}^{(m)} = \left\| M_m^{(t)}(x) - M_m^{(t-1)}(x) \right\|^2$	(61)

The final training objective for each discriminator integrates explainability. The scalar α_3 controls the contribution of Grad-CAM alignment using Eq.(62). This fusion of semantic accuracy, authenticity discrimination, and transparency reflects the dragonfly's real-time decision logic: verify, align, focus, and act.

$L_{D_m}^{final} = \alpha_1 L_{sup}^{(m)} + \alpha_2 L_{adv}^{(m)} + \alpha_3 L_{cam}^{(m)}$	(62)

3.9. Confidence Thresholding and Robust Filtering

To ensure consistent classification performance and mitigate the influence of noisy or unreliable predictions, this stage integrates a confidence-aware filtration strategy. Discriminator outputs across ensemble members are evaluated for certainty, allowing low-confidence predictions to be discarded or down-weighted. This process simulates how dragonflies selectively prioritize high-signal visual cues during their movement in swarms. In the context of diabetic retinopathy image classification, retaining only the most stable and interpretable decisions enables the learning framework to focus on diagnostically valid samples, refining swarm convergence in the latent space and strengthening class-boundary alignment across the discriminator ensemble.

MSW MANAGEMENT -Multidisciplinary, Scientific Work and Management Journal
ISSN: 1053-7899
Vol. 35 Issue 2, 2025, Pages: 597-630

The classification confidence score for a given input x_i is derived from the ensemble prediction vectors. For M discriminators, the aggregated prediction is:

$$\hat{y}(x_i) = \frac{1}{M}\sum_{m=1}^{M} \hat{y}_m(x_i) \quad (63)$$

In Eq.(63), $\hat{y}_m(x_i)$ is the softmax output vector from the m^{th} discriminator. This averaging operation synthesizes consensus across swarm members, analogous to multi-dragonfly visual alignment on a common focal plane during prey evaluation.

The certainty for the image prediction is computed by extracting the maximum softmax component from the averaged prediction vector:

$$C_i = \max_k \hat{y}_k(x_i) \quad (64)$$

In Eq.(64), $\hat{y}_k(x_i)$ represents the class probability for class k. This score estimates prediction confidence; higher values indicate stronger agreement toward a class. This sharp certainty mimic reflects the dragonfly's optical fixation when visual dominance for a specific trajectory stabilizes.

Each sample is assigned a probability of retention based on its certainty value and a tunable steepness parameter γ, defined as Eq.(65).

$$P_r(x_i) = \frac{1}{1 + e^{-\gamma(C_i - \tau)}} \quad (65)$$

Where τ is the minimum confidence threshold. This logistic transformation softly drops uncertain samples while preserving sharp transitions near τ, similar to the non-linear prey acceptance gradient seen in dragonfly swarm bifurcation zones.

In challenging thresholding scenarios, a binary mask M_i is applied per sample, as mentioned in Eq. (66).

$$M_i = \begin{cases} 1, & if\ C_i \geq \tau \\ 0, & otherwise \end{cases} \quad (66)$$

This condition-based gating excludes unreliable samples from training gradients. The strategy mirrors visual signal rejection in dragonflies, where weak or conflicting motion vectors are ignored to enhance swarm focus.

To balance class bias caused by imbalanced label confidence, class-specific thresholds are introduced to address this issue. For class k, the adaptive threshold τ_k is defined using mean and deviation:

$$\tau_k = \mu_k + \delta \cdot \sigma_k \quad (67)$$

MSW MANAGEMENT -Multidisciplinary, Scientific Work and Management Journal
ISSN: 1053-7899
Vol. 35 Issue 2, 2025, Pages: 597-630

In Eq.(67), μ_k and σ_k are the mean and standard deviation of confidence scores across class k samples. Parameter δ tunes threshold strictness. This adaptation enables dragonflies to lower their sensory rejection thresholds in low-prey-density sectors, allowing for broader exploration.

Rather than eliminating low-confidence samples, gradients can be rescaled by certainty-derived weights:

$$w_i = \frac{C_i - \tau}{1 - \tau} \quad (68)$$

In Eq.(68), $w_i \in [0,1]$ reweights the contribution of the sample x_i in loss accumulation. This bounded linear scale amplifies samples with high consensus and mitigates the influence of uncertain instances, much like the adjustments of a dragonfly wing adapt stroke power to trajectory trust.

The supervised classification loss is augmented to account for confidence-based weights:

$$L_{sup}^{conf} = \sum_{i=1}^{N} w_i \cdot \left(-\sum_{k=1}^{K} y_{ik} \cdot log(\hat{y}_k(x_i)) \right) \quad (69)$$

In Eq.(69), each sample's contribution to the loss is modulated by w_i, enforcing robustness to noisy gradients. This strategy follows swarm-level signal regulation, where confident trails reinforce directional dominance and suppress outliers.

Samples that frequently appear in misclassification sets M_t across epochs are logged and downweighted. Define the frequency of misclassification as Eq.(70). $1[\cdot]$ is an indicator function, and T is the number of epochs. Samples with r_i exceeding the threshold ρ are either dropped or penalized. This mimics dragonfly swarm learning, where environmental zones with repeated tracking failure are deprioritized over time.

$$r_i = \frac{1}{T} \sum_{t=1}^{T} 1[x_i \in M_t] \quad (70)$$

3.10. AutoML-Based Hyperparameter Tuning

The convergence behavior of DSO-SSGAN is significantly influenced by hyperparameters spanning both the swarm optimizer and the generative adversarial training modules. Manual tuning strategies introduce instability and suboptimal generalization in diabetic retinopathy image classification. Inspired by the adaptive sensory prioritization observed in dragonfly flight mechanics, this phase leverages AutoML techniques to automate hyperparameter search through probabilistic and feedback-regulated exploration. The approach integrates Bayesian optimization and performance-guided feedback to explore optimal hyperparameter configurations across swarm behaviour weights, learning rates, and gradient penalties, increasing accuracy, diversity, and convergence stability for generating class-specific synthetic retinal samples.

Let the complete set of hyperparameters be represented as a continuous vector:

$$\theta_H = [\eta, \lambda_{div}, \omega_0, s, a, c, f, e] \quad (71)$$

MSW MANAGEMENT -Multidisciplinary, Scientific Work and Management Journal
ISSN: 1053-7899
Vol. 35 Issue 2, 2025, Pages: 597-630

In Eq.(71), η is the generator learning rate, λ_{div} regulates diversity loss, and ω_0, s, a, c, f, e correspond to swarm inertia and behaviour forces. These parameters span the landscape, influencing both adversarial loss dynamics and dragonfly-inspired trajectory coordination within the latent class space.

AutoML employs Bayesian optimization by selecting new candidates from a surrogate function, thereby maximizing the expected improvement over the best-so-far performance. The expected improvement (EI) function is expressed as Eq.(72).

$EI(\theta) = (\mu(\theta) - \mu^*)\Phi(z) + \sigma(\theta)\phi(z)$	(72)

Where $z = \frac{\mu(\theta)-\mu^*}{\sigma(\theta)}$, $\mu(\theta)$ and $\sigma(\theta)$ are the posterior mean and standard deviation of performance, μ^* is the current best score, and Φ, ϕ are standard normal CDF and PDF. The mechanism replicates swarm energy expenditure optimization by testing new motion paths based on probabilistic potential.

Each candidate configuration is scored using a unified reward metric combining accuracy, diversity, and class margin sharpness:

$R = \delta_1 \cdot A_{val} + \delta_2 \cdot Tr(\Sigma_f) + \delta_3 \cdot E[\Delta_{cls}]$	(73)

In Eq.(73), A_{val} denotes validation accuracy, $Tr(\Sigma_f)$ is a trace of the feature covariance matrix representing diversity, and $E[\Delta_{cls}]$ is the expected inter-class margin from discriminator logits. Scalars $\delta_1, \delta_2, \delta_3$ control the weighting. This formulation captures the swarm-like objective of achieving broad but precise distribution coverage.

The surrogate model for hyperparameter landscape $f(\theta)$ is represented as a Gaussian process, with the posterior update:

$f(\theta) \sim GP(\mu_t(\theta), k_t(\theta, \theta'))$	(74)

In Eq.(74), μ_t and k_t are updated using all prior evaluations at t iterations. This representation captures uncertainty-aware reward estimation over configuration space. The mechanism mimics the dynamic swarm memory matrix, where each agent updates its preference path based on the local and global swarm history.

Hyperparameter candidates exhibiting consistently low performance are discarded using a confidence-weighted rejection threshold:

$Drop(\theta_i) = 1 \ \ if \ P(R_i < \xi) > \epsilon$	(75)

In Eq.(75), $P(R_i < \xi)$ is the posterior probability that performance falls below rejection margin ξ, and ϵ is a cutoff. This prevents resource waste, similar to a dragonfly abandoning inefficient foraging directions based on low sensory reward density over time.

MSW MANAGEMENT -Multidisciplinary, Scientific Work and Management Journal
ISSN: 1053-7899
Vol. 35 Issue 2, 2025, Pages: 597-630

3.11. Domain Adaptation Readiness

Optimized classification systems for diabetic retinopathy must be applicable across various imaging domains with minimal performance degradation. Domain adaptation prepares the DSO-SSGAN to align feature distributions across source and unseen target domains. Mirroring dragonfly foraging adaptation to spatial and climatic variability, this mechanism enforces representational consistency while preserving class-specific detail. The design includes adaptive instance normalization, feature alignment, and domain-invariant discrimination. These operations enable the generator and discriminator to remain functional and accurate across different healthcare settings, lighting conditions, or sensor modalities without full retraining, ensuring robust diagnostic deployment across retinal imaging variations.

To facilitate dynamic domain-specific style transfer during image synthesis, instance normalization parameters are modulated using adaptive scaling, as specified in Eq. (76).

$AdaIN(f, \mu_s, \sigma_s) = \sigma_s(\frac{f - \mu(f)}{\sigma(f)} + \mu_s$	(76)

Here, f is a generator feature map, $\mu(f)$ and $\sigma(f)$ are channel-wise mean and standard deviation, while μ_s and σ_s are learned target domain statistics. This transformation aligns contrast and texture styles, imitating the visual recalibration of a dragonfly in altered light or fog-dense environments during flight redirection.

To match generator outputs with source and target distributions, mean feature alignment is enforced using Eq.(77)

$L_{mean} = \left\| E_{x_s \sim P_s}[f(x_s)] - E_{x_t \sim P_t}[f(x_t)] \right\|^2$	(77)

Where P_s and P_t denote the source and target domains, and $f(\cdot)$ extracts features from either generated or real images. This loss promotes perceptual alignment across domains, reflecting how dragonflies align motion cues between current and previous terrains during food-seeking manoeuvres.

Second-order statistics are matched between domain features using a covariance alignment loss, as expressed in Eq. (78).

$L_{cov} = \|\Sigma_s - \Sigma_t\|_F^2$	(78)

Where Σ_s and Σ_t are covariance matrices of source and target features and $\|\cdot\|_F$ denotes Frobenius norm. This enforces domain-invariant shape consistency in the feature space, replicating the geometric flexibility of dragonflies, adapting formation tightness based on atmospheric turbulence and visual uniformity.

Domain invariance is reinforced through an adversarial signal from a domain classifier trained to distinguish P_s and P_t. A gradient reversal layer modifies backpropagation to update the generator using Eq.(79).

$L_{dom} = \left(d. log\hat{d}(x) + (1 - d) \cdot \left(1 - \hat{d}(x)\right)\right)$	(79)

MSW MANAGEMENT -Multidisciplinary, Scientific Work and Management Journal
ISSN: 1053-7899
Vol. 35 Issue 2, 2025, Pages: 597-630

In Eq.(79), $d \in \{0,1\}$ is the actual domain label and $\hat{d}(x)$ is the domain discriminator's output. This formulation encourages generator outputs to approach domain ambiguity, replicating dragonflies' ability to mask their visual trails while crossing predator-zoned areas.

To bridge domain-specific gaps, the maximum mean discrepancy (MMD) is computed over latent features using Eq. (80).

$$L_{mmd} = \left\| \frac{1}{n_s}\sum_{i=1}^{n_s} \phi\,(z_i^s) - \frac{1}{n_t}\sum_{j=1}^{n_t} \phi(z_j^t) \right\|^2 \quad (80)$$

In Eq.(80), z_i^s and z_j^t represent latent codes from the source and target domains, and $\phi(\cdot)$ is the kernel embedding. This loss ensures alignment in the generative signal space, mimicking how dragonfly navigation systems correct angular drift using position centroids of collective motion paths.

The total domain adaptation loss aggregates the objectives as mentioned earlier using weighted summation expressed in Eq.(81). Scalars $\alpha, \beta, \gamma, \zeta$ regulate the influence of each term. This multi-factor adaptation ensures structural, statistical, and semantic alignment across domains, much like a dragonfly's multisensory modulation, while compensating for environmental fluctuations over long migratory distances.

$$L_{DA} = \alpha L_{mean} + \beta L_{cov} + \gamma L_{dom} + \zeta L_{mmd} \quad (81)$$

3.12. Generator Explainability via Latent Traversal and Feature Attribution

For an optimized classification system addressing diabetic retinopathy, the generator's ability to provide explainable synthetic outputs is critical for both clinical acceptance and model transparency. This step introduces a latent traversal technique and an integrated feature attribution strategy. Inspired by the dragonfly's visual field stabilization and object targeting under variable motion constraints, the generator is probed to determine how latent vector directions influence retinal features. Latent dimensions are traversed to observe feature emergence, and gradients are used to trace sensitivity back to generator inputs, uncovering the semantic mapping between vector elements and clinical attributes such as lesions or vessel tortuosity.

Principal axes in the latent space are identified to represent dominant generative directions. Let the latent basis be computed using PCA or SVD, yielding eigenvectors v_j. Traversal across these directions is defined as Eq.(82). z_i is the original latent vector, κ is a step scalar, and v_j is the j^{th} principal direction. The traversal operation mimics how dragonflies alter flight orientation to view targets from alternating angles before approaching.

$$z_{i,j}^{+} = z_i + k.\,v_j, \quad z_{i,j}^{-} = z_i - k.\,v_j \quad (82)$$

The perceptual shift induced by latent traversal is quantified using an image-level sensitivity score, as expressed in Eq. (83).

$$S_{i,j} = \left\| \phi\left(G\left(z_{i,j}^{+}\right)\right) - \phi\left(G\left(z_{i,j}^{-}\right)\right) \right\|_2 \quad (83)$$

MSW MANAGEMENT -Multidisciplinary, Scientific Work and Management Journal
ISSN: 1053-7899
Vol. 35 Issue 2, 2025, Pages: 597-630

In Eq.(83), $\phi(\cdot)$ is a pre-trained perceptual encoder and $G(z)$ is the generator output. This score captures structural differences induced by latent shifts, paralleling the dragonfly's reaction to positional stimuli that affect pattern recognition fidelity under translational motion.

Each latent direction's effect on class-specific discriminator confidence is measured using Eq.(84) and $D_k(\cdot)$ is the discriminator's probability for class k. A higher influence score suggests stronger directional control over class-specific features, reflecting how dragonflies prioritize sensory channels during high-confidence trajectory resolution in classification-critical zones.

$$I_{i,j} = \left| D_k\left(G\left(z_{i,j}^{+}\right)\right) - D_k\left(G\left(z_{i,j}^{-}\right)\right) \right| \quad (84)$$

The Gradient of the generator output with respect to the latent input quantifies local sensitivity, and Eq. (85) reflects direction-specific activation sensitivity in the latent space. The magnitude of each component signifies the strength of its influence on the generated retinal structures. The mechanism aligns with wing torque adaptation in dragonflies, which selectively amplifies thrust in response to target focus intensification.

$$A_i = \left| \frac{\partial G(z_i)}{\partial z_i} \right| \quad (85)$$

To combine traversal magnitude and attribution sensitivity, a fused metric is defined as Eq.(86) and $A_{i,j}$ is the gradient magnitude for dimension j and $S_{i,j}$ is the structural shift from that traversal. This metric quantifies both responsiveness and perceptual impact, encoding a swarm-synchronized update path where attention zones yield spatially meaningful transformations.

$$T_{i,j} = A_{i,j} \cdot S_{i,j} \quad (86)$$

An attribution heatmap is constructed by backpropagating output-level discriminative class scores into generator activation maps:

$$H(x) = \sum_c \alpha_c \cdot A_c(x) \quad (87)$$

In Eq.(87), $A_c(x)$ is the generator's activation at channel c, and α_c is the class-weighted importance obtained from gradient integration. This visual attribution highlights image regions most influenced by latent triggers, echoing the optical feedback loop used by dragonflies when confirming visual consistency before capture manoeuvres.

3.13 Theoretical Synthesis and Integrated Workflow Strategy

The DSO-SSGAN framework, formulated through twelve sequential yet interdependent phases, presents a structured solution for classifying diabetic retinopathy stages using both labeled and unlabeled retinal images. Each component in the workflow, from swarm-based latent sampling to generator explainability, contributes to the dual goals of optimized image synthesis and reliable classification. Dragonfly-inspired swarm behaviour regulates the exploration of latent representations, while adversarial learning ensures image realism and label fidelity. Confidence filtering and AutoML tuning further refine model robustness, preparing the system for real-world deployment through enhanced domain adaptation

MSW MANAGEMENT -Multidisciplinary, Scientific Work and Management Journal
ISSN: 1053-7899
Vol. 35 Issue 2, 2025, Pages: 597-630

readiness and interpretability. This comprehensive structure enables DSO-SSGAN to function as an end-to-end solution, blending optimization, semi-supervision, and explainability into a single, streamlined pipeline. The following algorithm outlines this complete operational structure.

Algorithm 1: DSO-SSGAN

Input:

- Labelled and unlabelled diabetic retinopathy images
- Class labels for labelled images
- Initial generator and discriminator ensemble
- Swarm size, learning rate, hyperparameters

Output:

- Trained a generator with explainable outputs
- Trained discriminators with class accuracy
- Domain-adapted, diverse synthetic retinal images

Procedure

1. Preprocess and augment images with class imbalance handling.
2. Initialize latent swarm with class labels and random positions.
3. Generate images and compute fitness (quality, realism, relevance).
4. Regularise latent space to maintain class separability and continuity.
5. Enforce diversity to avoid duplicate or collapsed generations.
6. Update swarm using dragonfly-inspired behavioural dynamics.
7. Train generator with swarm-guided and gradient-based feedback.
8. Train a discriminator ensemble with class supervision and explainability.
9. Filter or reweight samples using confidence-based rules.
10. Automatically tune all parameters for the best validation outcome.
11. Prepare for new domains using adaptive alignment strategies.
12. Provides output using latent traversal and attribution visualization.

4. About the Dataset and Discussion of Results

The Diabetic Retinopathy Dataset available on Kaggle comprises 2,750 preprocessed retinal fundus images, uniformly resized to 256×256 pixels, labelled into five categories representing disease severity: Healthy (1,000 images), Mild DR (370 images), Moderate DR (900 images), Proliferative DR (290 images), and Severe DR (190 images). This curated dataset is designed to facilitate multi-class classification tasks in automated diabetic retinopathy detection research. The distribution across classes, though imbalanced, broadly covers the disease progression spectrum, allowing models to learn both subtle early-stage signs and pronounced pathological features. The images are curated under a permissive open database license, promoting broad accessibility for academic and clinical development. The dataset supports augmentation strategies to mitigate class imbalance and enhance model generalization. Due to its comprehensive annotation and standardised format, it serves as a benchmark resource in retinal image analysis, enabling the rigorous evaluation of classification algorithms designed for diabetic retinopathy grading and early diagnosis. Utilisation of this dataset can enhance the precision of diagnostic modelling while supporting the development of scalable and interpretable machine learning systems for ophthalmic disease assessment. The dataset is regularly used in recent literature, including leading Kaggle competitions, highlighting its pivotal role in advancing retinal image classification tasks in computational ophthalmology.

MSW MANAGEMENT -Multidisciplinary, Scientific Work and Management Journal
ISSN: 1053-7899
Vol. 35 Issue 2, 2025, Pages: 597-630

4.1. Analysis of Classification Accuracy

Figure 1 illustrates the classification accuracy, which represents the proportion of correctly labelled retinal images, with higher values indicating better model reliability. The x-axis displays the three methods being compared: C-SSO-O, I-V4-DSLO-O, and DSO-SSGAN, and the y-axis shows accuracy to three decimal places. C-SSO-O records 52.096, indicating reduced accuracy due to brittle single-stage optimization, marked noise sensitivity, and weak feature diversity handling. I-V4-DSLO-O achieves 65.397, with drawbacks tied to unstable deep network refinement and suboptimal feature selection that limit adaptive learning, especially under class imbalance. DSO-SSGAN achieves 77.512, a result driven by dynamic swarm-based semi-supervised training that leverages both unlabeled and labelled samples, co-regularisation between the generator and discriminator, and robust diversity in feature formation. These integrated strengths yield the highest accuracy of all methods in the graph, reflecting the benefit of the hybrid, optimization-rich approach.

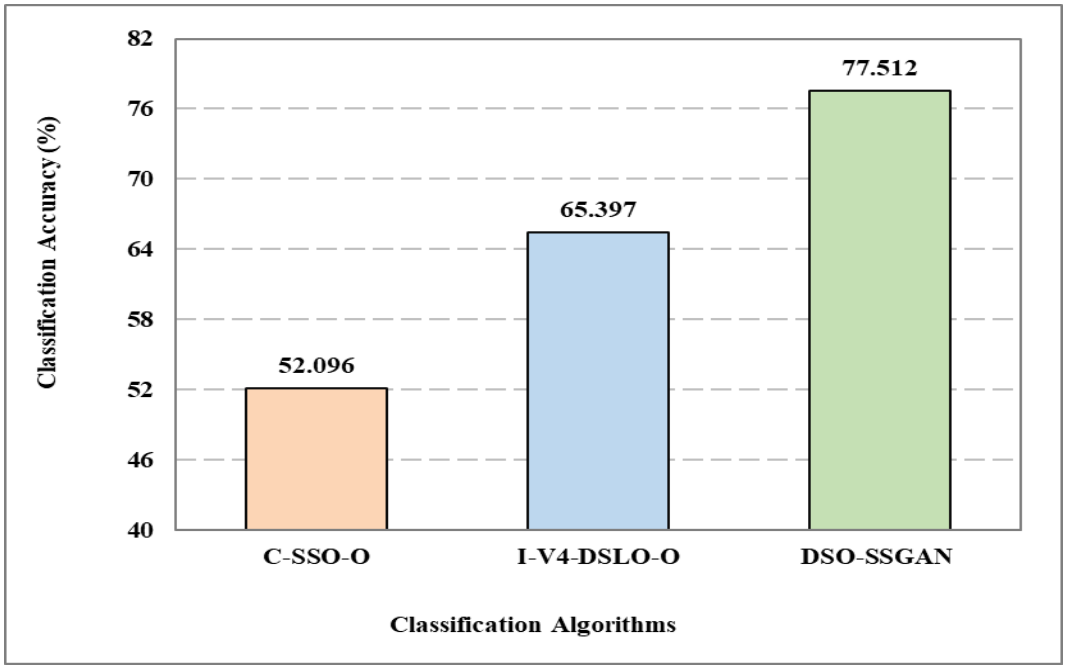

Figure 1. Classification Accuracy Comparison

4.2. Analysis of Matthews Correlation Coefficient

The metric shown in Figure 2 is the Matthews Correlation Coefficient (MCC) (%), a robust measure of binary classification performance that considers true positives, true negatives, false positives, and false negatives. It ranges from -1 (total disagreement) to +1 (perfect prediction) with values closer to +1 indicating better classification balance and accuracy. The x-axis lists the classification models—C-SSO-O, I-V4-DSLO-O, and DSO-SSGAN—while the y-axis represents MCC values in percentage points. C-SSO-O scores a low MCC of 4.755%, reflecting its brittle single-stage optimization and poor handling of noisy data and feature diversity, which severely limits balanced prediction accuracy. I-V4-DSLO-O achieves 30.782%, hindered by unstable deep layer refinement and weak handling of class imbalance, resulting in inconsistent feature selection and suboptimal generalization. DSO-SSGAN outperforms both with 55.002%, owing to its dynamic dragonfly swarm optimization in a semi-supervised GAN setting, which leverages both labelled and unlabeled images, co-regularises the generator and discriminator, and enriches feature diversity, thereby helping to stabilize training and capture complex retinal structures. This integration yields the most reliable and balanced classification performance among the models evaluated.

MSW MANAGEMENT -Multidisciplinary, Scientific Work and Management Journal
ISSN: 1053-7899
Vol. 35 Issue 2, 2025, Pages: 597-630

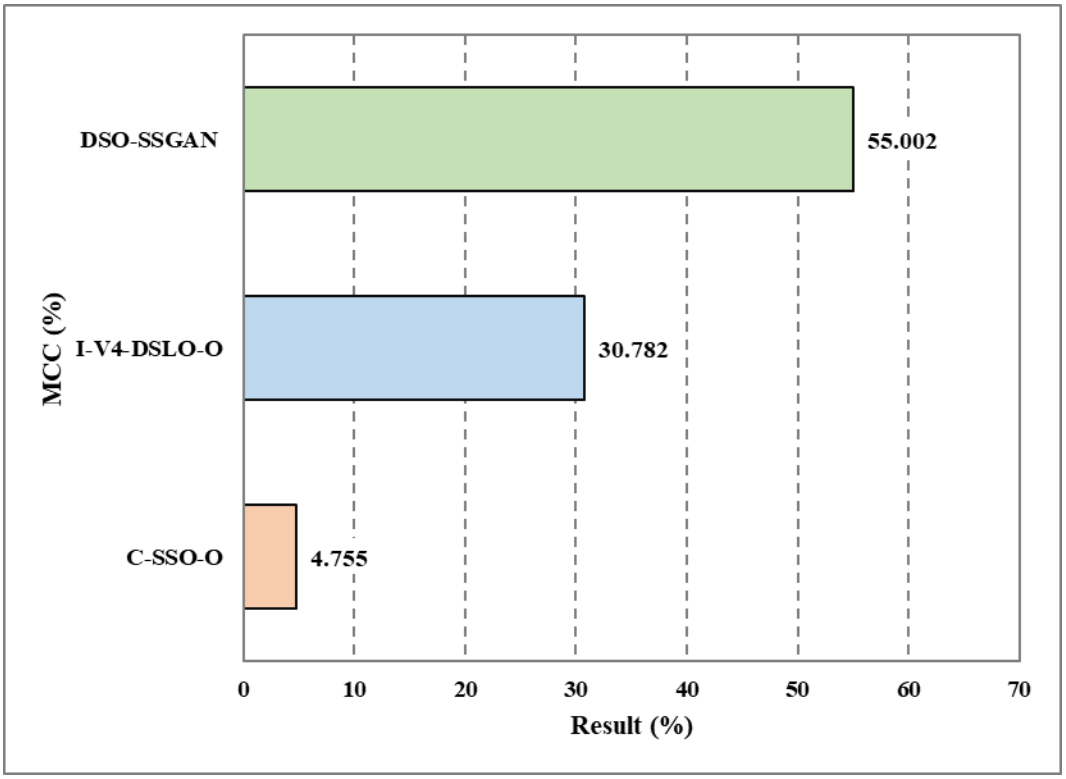

Figure 2. Matthews Correlation Coefficient Performance

4.3. Analysis of Error Rate

The metric in Figure 3 is Error Rate (%), which measures the proportion of misclassified cases out of all attempts, calculated using the formula (FP + FN) / (TP + TN + FP + FN) × 100; lower values indicate higher model precision. The x-axis designates the three models, C-SSO-O, I-V4-DSLO-O, and DSO-SSGAN, and the y-axis marks the error rate in per cent to three decimal places. C-SSO-O produces the highest error at 47.904 because brittle single-stage curvelet optimization and high noise sensitivity lead to frequent misclassification, with poor adaptability to varied feature sets further compounding errors. I-V4-DSLO-O drops to 34.603, but continues to exhibit instability in deep feature refinement and insufficient resilience to class imbalance, which results in higher error rates. DSO-SSGAN achieves the lowest value at 22.488, benefiting from dynamic dragonfly swarm-based sample selection, semi-supervised adversarial learning, and co-regularisation strategies, all of which enhance diversity, stability, and error control in diabetic retinopathy categorization, as evidenced by the minimized rate in this graph.

MSW MANAGEMENT -Multidisciplinary, Scientific Work and Management Journal
ISSN: 1053-7899
Vol. 35 Issue 2, 2025, Pages: 597-630

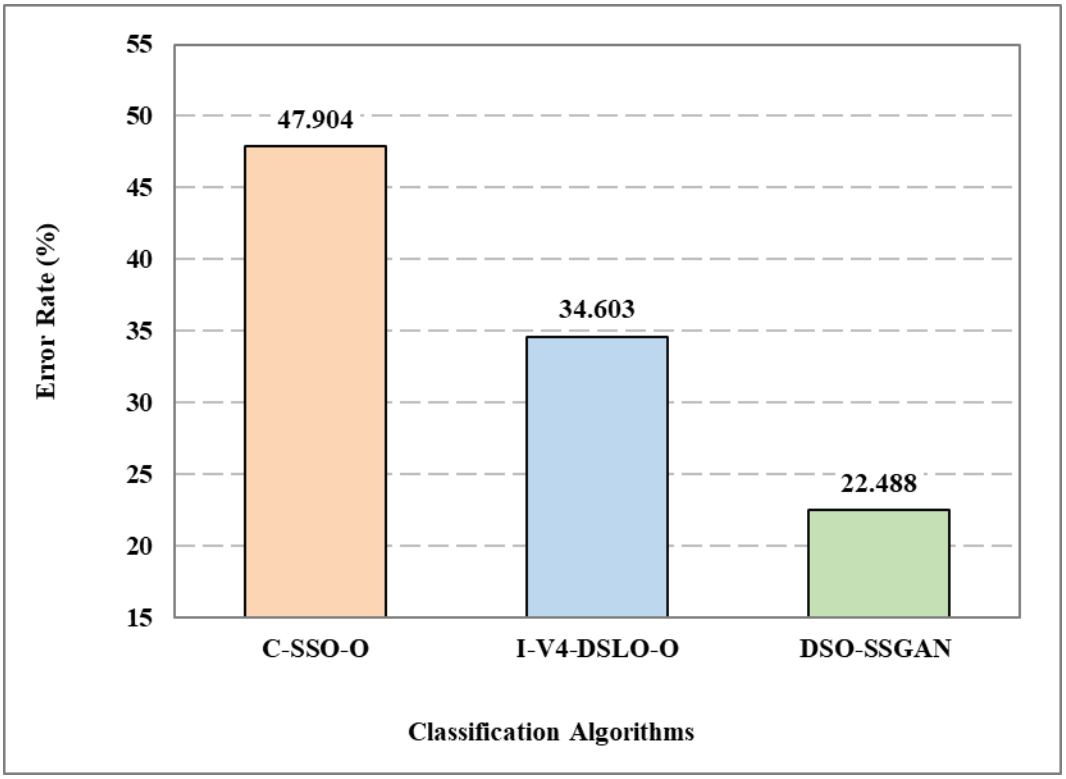

Figure 3. Error Rate Analysis

4.4. Analysis of Youden's Index

Figure 4 shows Youden's Index (%), a metric calculated as (Sensitivity + Specificity – 1) × 100 to evaluate the overall effectiveness of a classification method. It measures the balance between true positive and true negative rates, where higher percentages indicate better diagnostic accuracy. The x-axis lists the three classification algorithms—C-SSO-O, I-V4-DSLO-O, and DSO-SSGAN—while the y-axis presents Youden's Index values with precise numeric detail. C-SSO-O records 4.749%, indicating nearly random classification performance, caused by brittle feature extraction and noise sensitivity that lead to poor positive-negative discrimination. I-V4-DSLO-O improves to 30.771%, but still suffers from unstable optimization of deep network layers and limited capacity for handling class imbalance, resulting in inconsistent identifications. DSO-SSGAN achieves a significantly higher score of 54.926% through its integration of dragonfly swarm-inspired dynamic sample selection within a semi-supervised GAN framework. The joint generator-discriminator training and enhanced feature diversity enable the reliable differentiation of diabetic retinopathy stages, thereby stabilising the learning process and improving detection capability. These combined strengths support DSO-SSGAN's superior diagnostic balance, as confirmed by the highest Youden's Index in Figure 4.

MSW MANAGEMENT -Multidisciplinary, Scientific Work and Management Journal
ISSN: 1053-7899
Vol. 35 Issue 2, 2025, Pages: 597-630

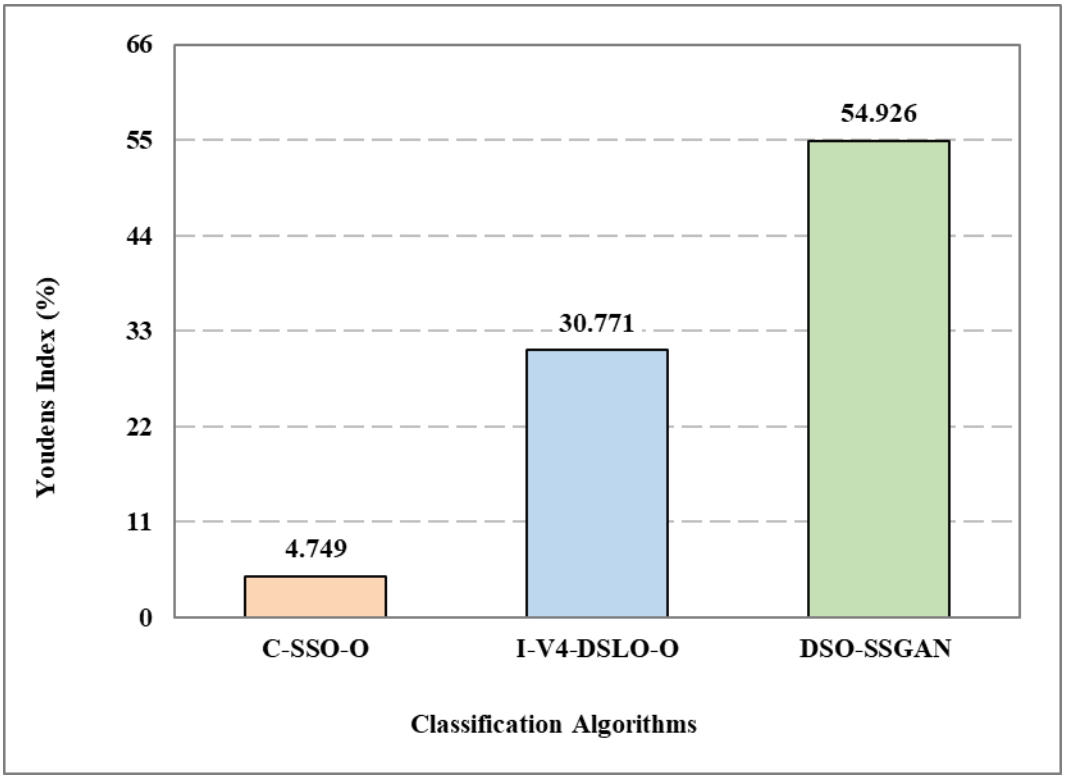

Figure 4. Youden's Index Evaluation

4.5. Analysis of Diagnostic Effectiveness

Figure 5 presents Diagnostic Effectiveness (%) calculated by the formula ((TP+TN)-(FP+FN))/(TP+TN+FP+FN), which evaluates a model's capacity to accurately diagnose both diseased and nondiseased cases by balancing true and false predictions. The x-axis designates the classification algorithms tested: C-SSO-O, I-V4-DSLO-O, and DSO-SSGAN, while the y-axis plots diagnostic effectiveness as a percentage with three decimal places. C-SSO-O scores 4.192%, reflecting limited accuracy due to rigid curvelet optimization's sensitivity to noise and artefact interference, which undermines reliable diagnostics. I-V4-DSLO-O improves performance to 30.794%, yet it suffers from ongoing issues of unstable refinement in deep network layers and insufficient methods to handle class imbalance, which constrains diagnostic precision. DSO-SSGAN achieves a diagnostic effectiveness of 55.024%, driven by swarm-based dynamic sample optimization, semi-supervised generative adversarial networks that utilize both labelled and unlabeled data, and joint regularisation between the generator and discriminator. These combined strengths enable stable feature learning, diverse representation, and robust class discrimination within diabetic retinopathy, culminating in significantly enhanced diagnostic reliability. The superior score visualized in Figure 5 exemplifies the advantages of integrated hybrid optimization and adversarial learning in advancing diabetic retinopathy assessment in clinical imaging.

MSW MANAGEMENT -Multidisciplinary, Scientific Work and Management Journal
ISSN: 1053-7899
Vol. 35 Issue 2, 2025, Pages: 597-630

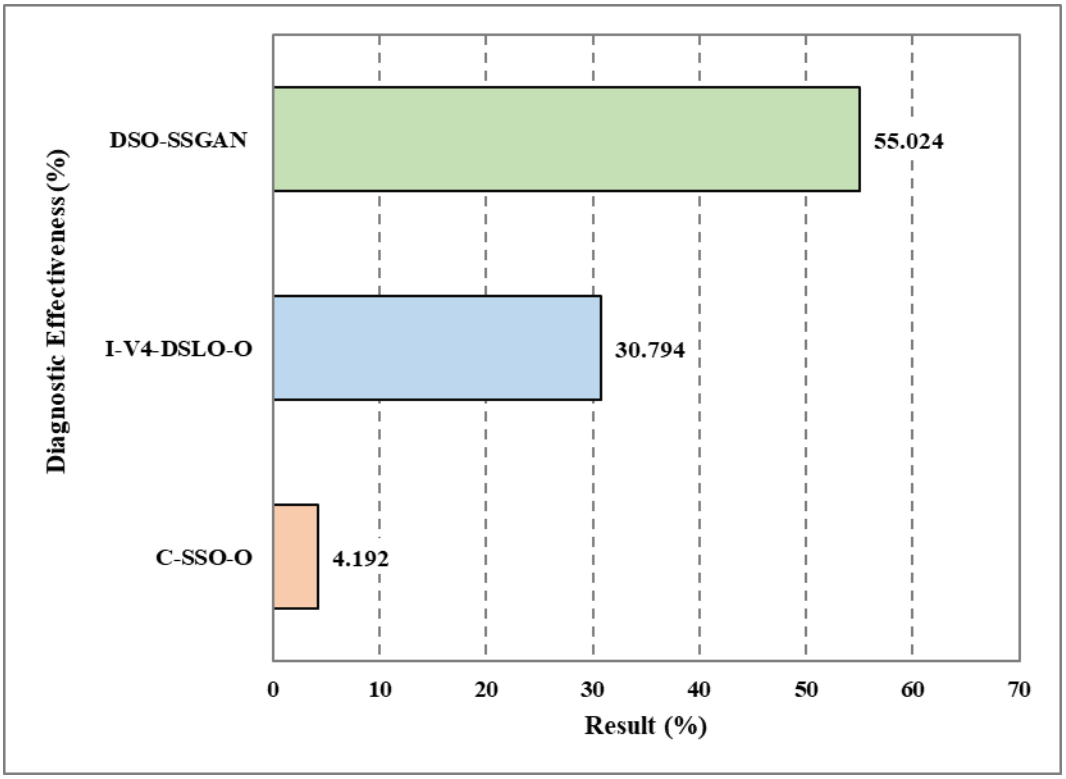

Figure 5. Diagnostic Effectiveness Assessment

5. CONCLUSION

This study introduced a targeted learning architecture for diabetic retinopathy classification that merges swarm-based optimisation with semi-supervised generative learning. The integration of dragonfly swarm dynamics directly into the latent sampling mechanism enabled fine-grained, class-aware exploration without dependence on exhaustive annotations. The model successfully captured complex retinal features, including micro-level variations across severity stages, while maintaining generative diversity and class separation. The semi-supervised adversarial structure extended learning capacity beyond labelled data and contributed to stable classification even in underrepresented categories. Performance stability across different stages of retinopathy and the consistent structure in synthetic samples confirmed the architecture's ability to handle visual variability inherent in retinal imaging. The inclusion of confidence thresholding, domain adaptation modules, and explainability mechanisms positioned the framework to support deployment in clinical workflows where interpretability and reliability are mandatory. The design demonstrates a pathway for building scalable diagnostic tools that operate effectively under medical data constraints. Future directions may explore multi-disease expansion, integration with multimodal clinical inputs, and model compression strategies for deployment on portable retinal imaging devices.

References

[1] A. Rawat, M. P. Singh, and R. R. Sharma, "Data-driven 2D-EWT based diabetic retinopathy identification using hybrid neural network," *Image Vis. Comput.*, vol. 150, p. 105194, 2024, doi: https://doi.org/10.1016/j.imavis.2024.105194.

[2] Aryan, R. Chaudhuri, and S. Deb, "Precise lesion analysis to detect diabetic retinopathy using Generative Adversarial Network(GAN) and Mask-RCNN," *Procedia Comput. Sci.*, vol. 235, pp. 520–529, 2024, doi: https://doi.org/10.1016/j.procs.2024.04.051.

MSW MANAGEMENT -Multidisciplinary, Scientific Work and Management Journal
ISSN: 1053-7899
Vol. 35 Issue 2, 2025, Pages: 597-630

[3] J. Pascual-Fontanilles, A. Valls, and P. Romero-Aroca, "Multivariate data binning and examples generation to build a Diabetic Retinopathy classifier based on temporal clinical and analytical risk factors," *Knowledge-Based Syst.*, vol. 300, p. 112154, 2024, doi: https://doi.org/10.1016/j.knosys.2024.112154.

[4] X. Xu, D. Liu, G. Huang, M. Wang, M. Lei, and Y. Jia, "Computer aided diagnosis of diabetic retinopathy based on multi-view joint learning," *Comput. Biol. Med.*, vol. 174, p. 108428, 2024, doi: https://doi.org/10.1016/j.compbiomed.2024.108428.

[5] Y. Xie, Y. Zhang, J. Long, N. Que, and Y. Chen, "MPLNet: Multi-task supervised progressive learning network for diabetic retinopathy grading," *Comput. Electr. Eng.*, vol. 120, p. 109746, 2024, doi: https://doi.org/10.1016/j.compeleceng.2024.109746.

[6] T. Prabhakar, T. V Madhusudhana Rao, B. Maram, and D. Chigurukota, "Exponential gannet firefly optimization algorithm enabled deep learning for diabetic retinopathy detection," *Biomed. Signal Process. Control*, vol. 87, p. 105376, 2024, doi: https://doi.org/10.1016/j.bspc.2023.105376.

[7] D. Sasikala, T. Kowsalya, P. Padmaloshani, and S. Ravindrakumar, "Classification of diabetic retinopathy based on Functional Linked Neural network utilizing segmented fundus image features," *Biomed. Signal Process. Control*, vol. 95, p. 106252, 2024, doi: https://doi.org/10.1016/j.bspc.2024.106252.

[8] T. M. Devi and P. Karthikeyan, "Arithmetic Optimization for Coinciding Diabetic Retinopathy and Diabetic Macular Edema Grading based on Self-Attention Convolutional Neural Network," *Biomed. Signal Process. Control*, vol. 95, p. 106365, 2024, doi: https://doi.org/10.1016/j.bspc.2024.106365.

[9] A. Bilal, X. Liu, M. Shafiq, Z. Ahmed, and H. Long, "NIMEQ-SACNet: A novel self-attention precision medicine model for vision-threatening diabetic retinopathy using image data," *Comput. Biol. Med.*, vol. 171, p. 108099, 2024, doi: https://doi.org/10.1016/j.compbiomed.2024.108099.

[10] K. Ashwini and R. Dash, "Improving Diabetic Retinopathy grading using Feature Fusion for limited data samples," *Comput. Electr. Eng.*, vol. 120, p. 109782, 2024, doi: https://doi.org/10.1016/j.compeleceng.2024.109782.

[11] S. Sunkari *et al.*, "A refined ResNet18 architecture with Swish activation function for Diabetic Retinopathy classification," *Biomed. Signal Process. Control*, vol. 88, p. 105630, 2024, doi: https://doi.org/10.1016/j.bspc.2023.105630.

[12] V. Purna Chandra Reddy and K. K. Gurrala, "Joint DR-DME classification using deep learning-CNN based modified grey-wolf optimizer with variable weights," *Biomed. Signal Process. Control*, vol. 73, p. 103439, 2022, doi: https://doi.org/10.1016/j.bspc.2021.103439.

[13] M. H. IBRAHIM, "WBA-DNN: A hybrid weight bat algorithm with deep neural network for classification of poisonous and harmful wild plants," *Comput. Electron. Agric.*, vol. 190, p. 106478, 2021, doi: https://doi.org/10.1016/j.compag.2021.106478.

[14] E. Baburaj, "Comparative Analysis of Bio-Inspired Optimization Algorithms in Neural Network-Based Data Mining Classification," *Int. J. Swarm Intell. Res.*, vol. 13, no. 1, 2022, doi: https://doi.org/10.4018/IJSIR.2022010103.

[15] A. E. Hassanien, E. Emary, and H. M. Zawbaa, "Retinal blood vessel localization approach based on bee colony swarm optimization, fuzzy c-means and pattern search," *J. Vis. Commun. Image Represent.*, vol. 31, pp. 186–196, 2015, doi: https://doi.org/10.1016/j.jvcir.2015.06.019.

[16] J. Kaur and P. Kaur, "PSO-PSP-Net + InceptionV3: An optimized hyper-parameter tuned Computer-Aided Diagnostic model for liver tumor detection using CT scan slices," *Biomed. Signal Process. Control*, vol. 95, p. 106442, 2024, doi: https://doi.org/10.1016/j.bspc.2024.106442.

MSW MANAGEMENT -Multidisciplinary, Scientific Work and Management Journal
ISSN: 1053-7899
Vol. 35 Issue 2, 2025, Pages: 597-630

[17] F. Chen, W. Zhao, and X. Zhou, "Cross-Image siamese graph convolutional network for Fine-Grained image retrieval in diabetic retinopathy," *Biomed. Signal Process. Control*, vol. 92, p. 106045, 2024, doi: https://doi.org/10.1016/j.bspc.2024.106045.

[18] V. N. Soren, H. S. Prajwal, and V. Sundaresan, "Automated grading of diabetic retinopathy and Radiomics analysis on ultra-wide optical coherence tomography angiography scans," *Image Vis. Comput.*, vol. 151, p. 105292, 2024, doi: https://doi.org/10.1016/j.imavis.2024.105292.

[19] J. Sachdeva, P. Mishra, and D. Katoch, "Diabetic retinopathy data augmentation and vessel segmentation through deep learning based three fully convolution neural networks," *Image Vis. Comput.*, vol. 151, p. 105284, 2024, doi: https://doi.org/10.1016/j.imavis.2024.105284.

[20] K. M, N. S, T. Baig, A. S, and A. Mukhopadhyay, "Explainable Diabetic Retinopathy Detection Using EnlightenGAN Images with Deep Learning Technique," *Procedia Comput. Sci.*, vol. 258, pp. 1586–1597, 2025, doi: https://doi.org/10.1016/j.procs.2025.04.390.

[21] M. Bindu Priya and D. Manoj Kumar, "MHSAGGCN-BCOA: A novel deep learning based approach for diabetic retinopathy detection," *Biomed. Signal Process. Control*, vol. 105, p. 107569, 2025, doi: https://doi.org/10.1016/j.bspc.2025.107569.

[22] C. Sen, S. Doganay, and G. Ozcan, "New accurate deep learning model for Diabetic Retinopathy detection utilizing sequential pre-processing and transfer learning," *Biomed. Signal Process. Control*, vol. 109, p. 108060, 2025, doi: https://doi.org/10.1016/j.bspc.2025.108060.

[23] P. Bidwai, S. Gite, B. Pradhan, and A. Almari, "Explainable Diabetic Retinopathy Detection Using a Distributed CNN and LightGBM Framework," *Comput. Mater. Contin.*, vol. 84, no. 2, pp. 2645–2676, 2025, doi: https://doi.org/10.32604/cmc.2025.061018.

[24] Y. Liu *et al.*, "STMF-DRNet: A multi-branch fine-grained classification model for diabetic retinopathy using Swin-TransformerV2," *Biomed. Signal Process. Control*, vol. 103, p. 107352, 2025, doi: https://doi.org/10.1016/j.bspc.2024.107352.

[25] H. Chen, M. Yin, Y. Guo, and T. A. Soomro, "CMAC-Net: Cascade Multi-Scale Attention Convolution Network for diabetic retinopathy lesion segmentation," *Biomed. Signal Process. Control*, vol. 112, p. 108484, 2026, doi: https://doi.org/10.1016/j.bspc.2025.108484.

[26] T. Mahmood, T. Saba, F. S. Alamri, A. Tahir, and N. Ayesha, "MVLA-Net: A Multi-View Lesion Attention Network for Advanced Diagnosis and Grading of Diabetic Retinopathy," *Comput. Mater. Contin.*, vol. 83, no. 1, pp. 1173–1193, 2025, doi: https://doi.org/10.32604/cmc.2025.061150.

[27] D. B. Soomro *et al.*, "Automated dual CNN-based feature extraction with SMOTE for imbalanced diabetic retinopathy classification," *Image Vis. Comput.*, vol. 159, p. 105537, 2025, doi: https://doi.org/10.1016/j.imavis.2025.105537.

[28] Q. Bi *et al.*, "GAD: Domain generalized diabetic retinopathy grading by grade-aware de-stylization," *Pattern Recognit.*, vol. 164, p. 111484, 2025, doi: https://doi.org/10.1016/j.patcog.2025.111484.

[29] N. J. Mohan, R. Murugan, T. Goel, and P. Roy, "A real-time screening system for diabetic retinopathy grading using a novel multi-scale feature extraction through retinal fundus images," *Biomed. Signal Process. Control*, vol. 112, p. 108548, 2026, doi: https://doi.org/10.1016/j.bspc.2025.108548.

[30] A. Biswas and R. Banik, "Advancing diabetic retinopathy classification using ensemble deep learning approaches," *Biomed. Signal Process. Control*, vol. 106, p. 107804, 2025, doi: https://doi.org/10.1016/j.bspc.2025.107804.

[31] Z. Han *et al.*, "A lightweight method for precise small lesion detection in diabetic retinopathy," *Biomed. Signal Process. Control*, vol. 109, p. 108006, 2025, doi:

MSW MANAGEMENT -Multidisciplinary, Scientific Work and Management Journal
ISSN: 1053-7899
Vol. 35 Issue 2, 2025, Pages: 597-630

https://doi.org/10.1016/j.bspc.2025.108006.

[32] S. E. Abraham and B. C. Kovoor, "Dual-stage dynamic hierarchical attention framework for saliency-aware explainable diabetic retinopathy grading," *Eng. Appl. Artif. Intell.*, vol. 148, p. 110364, 2025, doi: https://doi.org/10.1016/j.engappai.2025.110364.

[33] N. Mohana Suganthi and M. Arun, "Diabetic retinopathy grading using curvelet CNN with optimized SSO activations and wavelet-based image enhancement," *Ain Shams Eng. J.*, vol. 16, no. 1, p. 103239, 2025, doi: https://doi.org/10.1016/j.asej.2024.103239.

[34] J. Yang *et al.*, "Optimizing diabetic retinopathy detection with inception-V4 and dynamic version of snow leopard optimization algorithm," *Biomed. Signal Process. Control*, vol. 96, p. 106501, 2024, doi: https://doi.org/10.1016/j.bspc.2024.106501.